UNIVERSIDADE ESTADUAL PAULISTA – UNESP
Programa de Pós-Graduação em Ciência e Tecnologia de Materiais – POSMAT

Kleyton Torikai

Transistores orgânicos ultracompactos produzidos por autoenrolamento de nanomembranas

Sorocaba - SP
2018

Kleyton Torikai

Transistores orgânicos ultracompactos produzidos por autoenrolamento de nanomembranas

Dissertação de mestrado apresentada como requisito parcial para obtenção do título de Mestre no âmbito do Programa de Pós-Graduação em Ciência e Tecnologia de Materiais da Universidade Estadual Paulista "Júlio de Mesquita Filho".

Universidade Estadual Paulista "Júlio de Mesquita Filho"
Programa de Pós-Graduação em Ciência e Tecnologia de Materiais
Câmpus de Sorocaba

ORIENTADOR Prof. Dr. Carlos César Bof Bufon

Sorocaba - SP
2018

Torikai, Kleyton.
Transistores orgânicos ultracompactos produzidos por autoenrolamento de nanomembranas / Kleyton Torikai, 2018
72 f. : il.

Orientador: Carlos César Bof Bufon

Dissertação (Mestrado)–Universidade Estadual Paulista. Faculdade de Ciências, Bauru, 2018

1. Eletrônica orgânica. 2. Nanomembrana autoenrolada. 3. Transistor orgânico. 4. Dispositivos eletrônicos. 5. Eletrônica robusta I. Universidade Estadual Paulista. Faculdade de Ciências. II. Título.

UNIVERSIDADE ESTADUAL PAULISTA

Câmpus de Bauru

Faculdade de Ciências

ATA DA DEFESA PÚBLICA DA DISSERTAÇÃO DE MESTRADO DE KLEYTON TORIKAI, DISCENTE DO PROGRAMA DE PÓS-GRADUAÇÃO EM CIÊNCIA E TECNOLOGIA DE MATERIAIS , DA FACULDADE DE CIÊNCIAS - CÂMPUS DE BAURU.

Aos 04 dias do mês de dezembro do ano de 2018, às 09:00 horas, no(a) Auditório - UNESP/Sorocaba, reuniu-se a Comissão Examinadora da Defesa Pública, composta pelos seguintes membros: Prof. Dr. CARLOS CÉSAR BOF BUFON - Orientador(a) do(a) Laboratório Nacional de Nanotecnologia / Centro Nacional de Pesquisa em Energia e Materiais, Prof. Dr. LUCAS FUGIKAWA SANTOS do(a) IGCE / UNESP/Rio Claro (SP) , Prof. Dr. NILSON CRISTINO DA CRUZ do(a) Curso de Engenharia de Controle e Automação / Instituto de Ciência e Tecnologia/ UNESP/ Sorocaba, sob a presidência do primeiro, a fim de proceder a arguição pública da DISSERTAÇÃO DE MESTRADO de KLEYTON TORIKAI, intitulada **Transistores orgânicos ultracompactos produzidos por autoenrolamento de nanomembranas**. Após a exposição, o discente foi arguido oralmente pelos membros da Comissão Examinadora, tendo recebido o conceito final: APROVADO. Nada mais havendo, foi lavrada a presente ata, que após lida e aprovada, foi assinada pelos membros da Comissão Examinadora.

Prof. Dr. CARLOS CÉSAR BOF BUFON

Prof. Dr. LUCAS FUGIKAWA SANTOS

Prof. Dr. NILSON CRISTINO DA CRUZ

Este trabalho é dedicado a todos aqueles que me apoiaram ao longo de toda minha jornada para que eu pudesse chegar onde cheguei. Agradeço aos meus pais por todo o apoio e por me indicarem o caminho do conhecimento, para que hoje eu possa continuar seguindo esta jornada com minhas próprias pernas.

Também dedico este trabalho a todos os meus amigos pelo incentivo e apoio emocional. Agradeço, em especial, à Bianca por estar ao meu lado em todos os momentos e somando a todas as minhas conquistas. Muito obrigado.

AGRADECIMENTOS

Primeiramente, ao Centro Nacional de Pesquisa em Energia e Materiais (CNPEM)—em particular ao Laboratório Nacional de Nanotecnologia (LNNano)—pela oportunidade única de realizar esta pesquisa em suas instalações, sem as quais este estudo não seria possível.

A todo o grupo do laboratório de Dispositivos e Sistemas Funcionais (DSF). Em especial, ao orientador Carlos César Bof Bufon pelo apoio imensurável desde a concepção do projeto durante meu estágio da graduação até as correções e conselhos mesmo nas etapas finais do trabalho.

Ao Rafael, efetivamente coorientando este trabalho, e muitas vezes sendo meu conselheiro nas etapas mais complexas. Obrigado pelo carinho.

À Universidade Federal de São Carlos (UFSCar) pela oportunidade de uma formação superior gratuita e de qualidade em um curso tão ampliador como a Engenharia Física.

À Universidade Estadual Paulista "Júlio de Mesquita Filho" e a seu corpo docente, além da administração, por realizar seu trabalho com dedicação para que pudéssemos contar com uma formação de excelência.

O presente trabalho foi realizado com apoio da Coordenação de Aperfeiçoamento de Pessoal de Nível Superior - Brasil (CAPES) - Código de Financiamento 001.

Ressalta-se que as atividades de pesquisa aqui descritas estão inseridas no âmbito do projeto FAPESP Jovem Pesquisador (Proc. 2014/25979-2). À Fundação de Amparo à Pesquisa do Estado de São Paulo, obrigado.

"The things I once imagined would be my greatest achievements were only the first steps toward a future I can only begin to fathom."
(Jace Beleren)

RESUMO

A eletrônica orgânica mostrou-se comercialmente viável e competitiva, já sendo integrada em diversas tecnologias, e.g., displays flexíveis de OLED, painéis solares de grande área, dispositivos biocompatíveis/vestíveis, entre outras. A utilização de materiais orgânicos na fabricação de dispositivos eletrônicos explora vantagens como: flexibilidade mecânica, baixas temperaturas de processamento e possibilidade de se implementar melhorias e ajustes por meio de sínteses químicas. Entretanto, a eletrônica inorgânica já bem estabelecida ainda se destaca na área da eletrônica robusta, uma vez que os semicondutores orgânicos (OSCs) são bastante suscetíveis a condições mais extremas, como exposição a gases e radiação. Nesse sentido, a tecnologia de nanomembranas autoenroladas (NM) tem mostrado, nos últimos anos, um grande potencial na fabricação de dispositivos híbridos ultracompactos em uma arquitetura inédita para transistores orgânicos de filmes finos (OTFTs). A partir das técnicas tradicionais de microfabricação—fotolitografia, deposição de filmes finos—fabricou-se OTFTs sobre NMs que, uma vez liberadas do substrato através da remoção sistemática de uma camada de sacrifício, remodelam os dispositivos em uma arquitetura tubular tridimensional, reduzindo a área ocupada em aproximadamente 90% e protegendo os OSCs da área ativa do OTFT entre as múltiplas voltas das NMs. Assim, mostrou-se que a arquitetura confere novas propriedades aos OTFTs sem prejudicar as propriedades elétricas, suportando centenas de ciclos de compressão mecânica e mostrando-se resistentes a radiação ultravioleta e a vapores agressivos, como a amônia. Por fim, para validar a arquitetura de OTFT inédita, mostra-se que a estratégia utilizada é válida para diferentes OSCs e pode ser utilizada na fabricação de circuitos eletrônicos mais complexos a partir da associação de multiplos dispositivos, como o inversor aqui apresentado.

Palavras-chave: eletrônica orgânica, nanomembrana autoenrolada, transistor orgânico, microfabricação, dispositivos eletrônicos, eletrônica robusta.

ABSTRACT

In the recent years, the organic electronics' commercial viability and competitiveness became apparent, integrating a diversity of technologies, e.g., OLED flexible displays, large-area solar panels and biocompatible and wearable devices. The manufacturing of electronic devices with organic materials aims at exploiting inherent characteristics—mechanical flexibility, low processing temperatures and the potential of boosting and tailoring specific properties through chemical synthesis. However, there's still a gap between the well-established inorganic and the organic electronics concerning applications on rugged electronics, since the organic semiconductors (OSCs) are very susceptible to harsh conditions, e.g., exposition to UV radiation and gases. In this sense, recent advances on strained nanomembrane (NM) technology has shown enormous potential in the manufacturing of hybrid ultracompact devices in a novel organic thin-film transistor (OTFT) architecture. Through traditional microfabrication techniques—photolithography, thin-film deposition—OTFTs were fabricated on top of strained NMs, which promotes a reshaping of the devices into a 3D tubular architecture when released from the substrate. This process promotes a reduction in about 90% of the footprint area while protecting the OSC in the active area in between the multiple device windings. Therefore, the OTFTs have been endowed with new proprieties without loss of electric performance, while enduring hundreds of mechanical compression cycles and showing increased resilience against UV radiation and hazardous vapors, such as ammonia. Finally, to validate this novel OTFT architecture, this strategy has been shown to be valid for different OSCs and can be used to manufacture electronic circuits through the association of multiple devices, such as the inverter reported in this study.

Keywords: organic electronics, rolled-up nanomembrane, organic transistor, microfabrication, electronic devices, rugged electronics.

LISTA DE FIGURAS

Figura 1 – Ilustração de um dispositivo antes e após seu autoenrolamento. 26
Figura 2 – Esquemático de um OTFT com configuração de *gate* e contatos na base nos regimes de acumulação e depleção. 27
Figura 3 – Processo de reversão de imagem em fotorresistes positivos. 29
Figura 4 – Graphical abstract 34
Figura 5 – OTFT layout and layer composition. 37
Figura 6 – Electrical response of CuPc planar transistors (p-OTFTs) and rolled-up OTFTs (r-OTFTs). 38
Figura 7 – Mechanical properties of r-OTFTs. 41
Figura 8 – Evaluation of the r-OTFT self-encapsulation characteristics. 42
Figura 9 – Electrical characteristics of DNTT r-OTFTs. 45
Figura 10 – Gate leakage curves of CuPc transistores orgânicos de filmes finos (OTFTs) for both architectures. 49
Figura 11 – Unipolar p-type inverter based on CuPc OTFTs. 50
Figura 12 – Static compression of the CuPc r-OTFT by a round needle tip. 51
Figura 13 – Gate leakage current during static mechanical compression. 51
Figura 14 – Mercury lamp emission spectrum. Inset: absorption spectrum of CuPc thin-films adapted from Farag (2007). 52
Figura 15 – Gate leakage curves of DNTT OTFTs for both architectures. 52
Figura 16 – Main step-by-step fabrication schematics. 53
Figura 17 – Resultado de uma tentativa de autoenrolamento dos dispositivos de uma amostra do segundo lote de fabricação. 55
Figura 18 – Colapso do r-OTFT durante a secagem imediatamente após o processo de autoenrolamento. 57
Figura 19 – Processo de solda com fios de ouro (*wire bonding*) para a formação de circuitos. 57

LISTA DE TABELAS

Tabela 1 – CuPc r-OTFT electrical characteristics throughout mechanical stress. . 50
Tabela 2 – DNTT OTFTs electrical characteristics for both p- and r- architectures. 52

LISTA DE ABREVIATURAS E SIGLAS

ALD	deposição por camadas atômicas (*Atomic Layer Deposition*) 29, 36, 53
BSC	back sweep current 37, 44
CuPc	copper(II) phthalocyanine 37–44, 46, 48–51
DNTT	dinaphtho[2,3-*b*:2′,3′-*f*]thieno[3,2-*b*]thiophene 39, 44–46, 51, 52
EBPVD	deposição física por vapor assistida por feixe de elétrons (*electron-beam PVD*) 29, 53
NM	nanomembrana 25, 28, 35, 36, 39, 41, 43, 50, 53, 57
ODPA	octadecylphosphonic acid 36, 37, 46
OSC	semicondutor orgânico 25, 27, 34, 35, 37, 39, 42–44, 52, 54, 57
OTFT	transistor orgânico de filmes finos 26, 27, 33–39, 41–49, 51, 52, 57
p-OTFT	planar transistor 35–39, 42–44, 49, 50
PVD	deposição física por vapor 29
r-OTFT	rolled-up OTFT 35–47, 49, 50, 54, 55, 57
SAM	self-assembled monolayer 36, 44, 46
SS	subthreshold swing 37
UV	ultravioleta 28, 29, 33, 36, 37, 41–45, 47, 50

LISTA DE SÍMBOLOS

C_{I}	insulator specific capacitance 38, 48
I_{D}	corrente de dreno 37, 41, 43, 46
I_{G}	corrente de *gate* 37
I_{OFF}	corrente em estado desligado 37, 40
I_{ON}	corrente em estado ligado 37, 40
V_{DS}	tensão de fonte-dreno 37–40, 45, 46
V_{GS}	tensão de fonte-*gate* 37, 39, 40, 46
V_{TH}	device threshold voltage 38, 39, 43, 50, 51
V_{dd}	tensão de alimentação 49
g_{m}	transconductance 37, 40, 50, 51
μ	charge carrier mobility 37, 39, 40, 42, 43, 50, 51

SUMÁRIO

1 INTRODUÇÃO 25
1.1 Dispositivos baseados em nanomembranas autoenroladas . . . 26
1.2 Transistores orgânicos de filmes finos 26
1.3 Microfabricação 28
1.3.1 Fotolitografia 28
1.3.1.1 Fotorresiste 28
1.3.2 Fabricação de filmes finos 29

2 OBJETIVOS 31

3 ARTIGO ORIGINADOS DO TRABALHO 33
3.1 Low-Voltage, Flexible, and Self-Encapsulated Ultracompact Organic Thin-Film Transistors Based on Nanomembranes . . 33
3.1.1 Abstract 33
3.1.2 Main text 34
3.1.3 Associated Content 48
3.1.4 Author Information 48
3.1.5 Acknowledgments 48
3.1.6 Abbreviations 48
3.2 Supporting Information 49

4 DISCUSSÃO 55
4.1 Propriedades elétricas 56
4.2 Propriedades mecânicas 56
4.3 Aplicação em circuitos simples 56

5 CONCLUSÃO 59

REFERÊNCIAS 61

ANEXOS 67

ANEXO A – PAPER REUSE PERMISSION 69

1 INTRODUÇÃO

A utilização de materiais orgânicos para a fabricação de dispositivos eletrônicos, comumente conhecida como eletrônica orgânica, é uma realidade tecnológica que movimenta mais de U$ 23 bilhões ao ano na comercialização de produtos (DAS; HARROP, 2014). Atualmente, o dispositivo orgânico comercialmente mais bem-sucedido é o diodo emissor de luz (OLED, em inglês), presente na maioria dos displays de celulares e em alguns televisores. Acredita-se ainda, que a eletrônica orgânica poderá proporcionar num futuro próximo o desenvolvimento de diversas outras novas tecnologias, como painéis solares de grande área, displays flexíveis, dispositivos biocompatíveis para a interface homem/máquina, entre outras (SOMEYA; BAO; MALLIARAS, 2016). Esse avanço tecnológico seria possível devido a algumas vantagens que estes materiais apresentam em relação aos tradicionais materiais inorgânicos utilizados, como: baixo custo, versatilidade de síntese, flexibilidade, e processabilidade em baixas temperaturas e por solução. Por serem constituídos majoritariamente de hidrocarbonetos, materiais orgânicos são naturalmente mais baratos que seus análogos inorgânicos e também flexíveis. Além disso, a facilidade de processamento destes materiais implica diretamente em menores consumos de energia para fabricação em larga escala de dispositivos, redução do impacto ambiental causado pela produção industrial destes e, consequentemente, na redução dos custos totais de produção. A versatilidade de síntese, por sua vez, permite o ajuste de algumas propriedades destes materiais, como hidrofobicidade, condutividade, biocompatibilidade, porosidade, entre outras, de acordo com a aplicação desejada. Todas estas características fazem da eletrônica orgânica uma área de pesquisa atrativa e com potencial tecnológico crescente.

De acordo com o encontro Organic Electronics for a Better Tomorrow: Innovation, Accessibility and Sustainability, realizado há cerca de 2 anos nos Estados Unidos, e que contou com a presença de membros de diversos países, existem ainda inúmeros desafios a serem enfrentados a fim de aumentar sua comercialização e o desenvolvimento de novas tecnologias. Os principais desafios são: i) a melhoria dos processos de fabricação de dispositivos tridimensionais; ii) a aquisição de maior conhecimento de como materiais podem ser estruturados para garantir maior reprodutibilidade de dispositivos orgânicos em geral e; iii) a necessidade de se expandir a pesquisa no desenvolvimento de dispositivos multifuncionais (CHEMICAL SCIENCES AND SOCIETY SUMMIT (CS3), 2012). Além disso, dispositivos baseados em semicondutores orgânicos (OSCs) são mais suscetíveis a condições externas, como estresse mecânico e exposição a gases e radiação. Consequentemente, a manufatura deve levar em conta a robustez dos dispositivos para aplicações mais realistas (BASIRICÒ et al., 2017). Dentro deste contexto, este trabalho abordou os desafios mencionados utilizando uma plataforma baseada em nanomembranas autoenroladas (NMs) para a fabricação de dispositivos orgânicos (GRIMM et al., 2013; VERVACKE et al.,

2014).

1.1 Dispositivos baseados em nanomembranas autoenroladas

O autoenrolamento de filmes finos combina métodos *bottom-up* e *top-down* de nanofabricação para produção de diversas estruturas ultracompactas e tridimensionais . Nesta técnica, multicamadas de materiais com tensões mecânicas bem ajustadas são depositadas sobre uma camada de sacrifício. A remoção seletiva desta camada causa o relaxamento da tensão das multicamadas depositadas, que se autoenrolam, como ilustrado na Figura 1 (SCHMIDT; EBERL, 2001; MÜLLER et al., 2012; MATOVIC; JAKŠIĆ, 2009; FROETER et al., 2013; HUANG; MEI, 2012). Este método tem sido utilizado nos últimos anos na produção de vários dispositivos e sistemas tais como capacitores ultracompactos (BUFON et al., 2010; SHARMA et al., 2014; DENG et al., 2016; WANG et al., 2016; PETRINI et al., 2018), microbombas (SOLOVEV et al., 2011a), micromotores (SOLOVEV et al., 2011b), microcavidades óticas (WANG et al., 2017), indutores (HUANG et al., 2012; YU et al., 2015), heterojunções híbridas (BUFON et al., 2011; THURMER et al., 2010; BENDOVA et al., 2016; MERCES et al., 2017; OLIVEIRA et al., 2018), baterias (HUANG et al., 2017), sensores (MARTINEZ-CISNEROS et al., 2014; MÖNCH et al., 2011; VERVACKE et al., 2014), até mesmo um transistor de efeito de campo inorgânico (GRIMM et al., 2013).

Figura 1 – Ilustração de um dispositivo antes e após seu autoenrolamento.

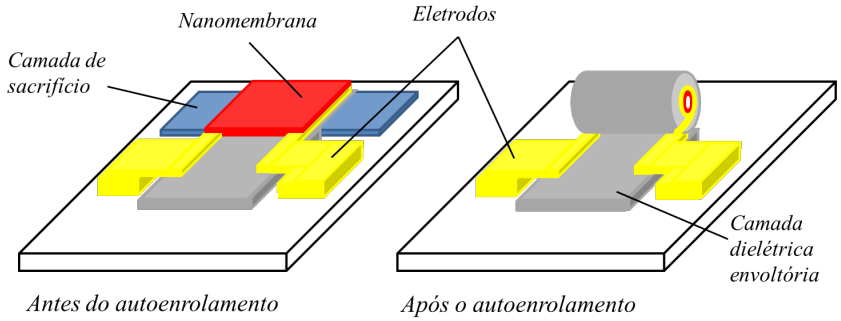

Fonte: de Oliveira (2016)

1.2 Transistores orgânicos de filmes finos

O transistor é um dos principais dispositivos eletrônicos da atualidade, estando presente em praticamente todas as aplicações tecnológicas. Suas funções básicas são a amplificação

e o chaveamento de um sinal elétrico. Quando a operação do transistor é determinada pela variação controlada do campo elétrico no dispositivo, diz-se que o transistor é de efeito de campo. A maioria dos transistores de efeito de campo existentes é baseada em materiais inorgânicos, principalmente o silício (REZENDE, 2004). A tecnologia de transistores orgânicos de filmes finos (OTFTs), entretanto, vem se desenvolvendo rapidamente, tendo seu desempenho melhorado 3–4 ordens de magnitude apenas 25 anos desde sua primeira aparição. Atualmente, OTFTs apresentam desempenhos que rivalizam àqueles obtidos para transistores de silício amorfo hidrogenado (a-Si:H) comumente utilizados em alguns displays. Essa equivalência de desempenho tem feito com que OTFTs começassem a ser integrados aos primeiros displays flexíveis desenvolvidos (SIRRINGHAUS, 2014).

O funcionamento de um OTFT depende de uma estrutura central nestes dispositivos do tipo metal/isolante/semicondutor. Através da aplicação de um campo elétrico apropriado ao longo desta estrutura pode-se controlar a corrente elétrica que flui no dispositivo, mais especificamente em uma região entre dois eletrodos denominada canal, como ilustrado na Figura 2.

Figura 2 – Esquemático de um OTFT com configuração de *gate* e contatos na base nos regimes de acumulação e depleção.

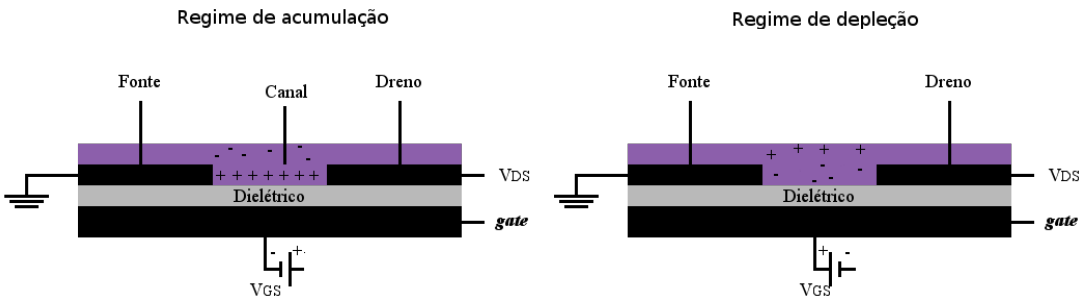

Fonte: o autor (2017)

Assim como em transistores inorgânicos, OTFTs podem ser classificados quanto ao sinal da carga elétrica de seus portadores, i.e., do tipo p (cargas positivas) e do tipo n (cargas negativas). Desta forma, ao se aplicar uma tensão negativa no *gate* de um dispositivo do tipo p, o campo elétrico através da estrutura do dispositivo causará o acúmulo de cargas positivas na interface isolante/semicondutor, formando a região do canal. Nesta condição diz-se que o dispositivo está em acumulação, ou ainda em um estado "ligado". Esta situação é análoga à aplicação de uma tensão de *gate* positiva em um dispositivo do tipo n. Em acumulação, a aplicação de uma tensão apropriada entre os eletrodos de fonte e dreno fará com que o dispositivo conduza corrente elétrica. Entretanto, a aplicação de uma tensão inapropriada ao *gate* do dispositivo, i.e., positiva para OTFTs do tipo p e negativa para OTFTs do tipo n, resultará na depleção dos portadores de carga na interface isolante/semicondutor. Nesta condição diz-se que o dispositivo está em um

estado "desligado". A utilização de OTFTs em aplicações práticas demanda a obtenção de dispositivos com estados de acumulação e depleção muito bem definidos, além de outras características importantes que estão discutidas mais adiante.

Escolheu-se os OTFTs como dispositivos-alvo para esta finalidade devido i) ao ineditismo deste tipo de dispositivo em configuração ultracompacta e ii) à relevância tecnológica para a eletrônica orgânica. Além disso, como muitos semicondutores orgânicos (OSCs) sofrem influência do ambiente externo—luz, umidade, gases, etc.—refletindo diretamente no desempenho elétrico (SATO et al., 2016; SCHOLZ et al., 2015), vemos nas nanomembranas autoenroladas (NMs) autoenroladas uma potencial plataforma para estudos de estabilidade destes dispositivos.

1.3 Microfabricação

A necessidade de se fabricar estruturas na escala do micrômetro deu origem a processos que conhecemos hoje como *microfabricação*. Nesta seção, são descritos os métodos utilizados na fabricação das amostras caracterizadas neste trabalho (FRANSSILA, 2010).

1.3.1 Fotolitografia

A fotolitografia, ou litografia ótica, é utilizada quando desejamos depositar ou remover filmes finos com um determinado padrão. A técnica se baseia na utilização de resinas fotossensíveis, ou fotorresiste, que têm suas propriedades afetadas por luz ultravioleta (UV), possibilitando a transferência de padrões desenhados em máscaras para o substrato. Neste trabalho, utilizou-se somente o modo de proximidade/contato, onde o padrão da máscara é transferido em escala 1:1 para o substrato.

Uma vez que o padrão desejado é transferido no fotorresiste, pode-se trabalhar na região exposta—seja depositando material ou removendo material. Após esse processo, realiza-se a remoção do fotorresiste (*lift-off*).

1.3.1.1 Fotorresiste

Os fotorresistes são resinas sintetizadas a partir de fenóis e formaldeídos contendo um composto fotoativo que reage quando exposto à radiação UV. Estes são classificados em dois tipos: fotorresistes positivos contém um composto fotoativo que aumenta a solubilidade alcalina após a exposição UV. E fotorresistes negativos contém um composto fotoativo que promove uma fotopolimerização durante a exposição, reduzindo a solubilidade da região exposta. Neste estudo, utilizamos um fotorresiste positivo, porém, realizamos um processo de reversão de imagem, onde a região exposta fica suscetível a uma reticulação polimérica (*crosslink*) quando realizado um tratamento térmico. Assim, a região exposta torna-se menos solúvel e já não contendo o composto fotoativo. Assim, após uma segunda

Figura 3 – Processo de reversão de imagem em fotorresistes positivos.

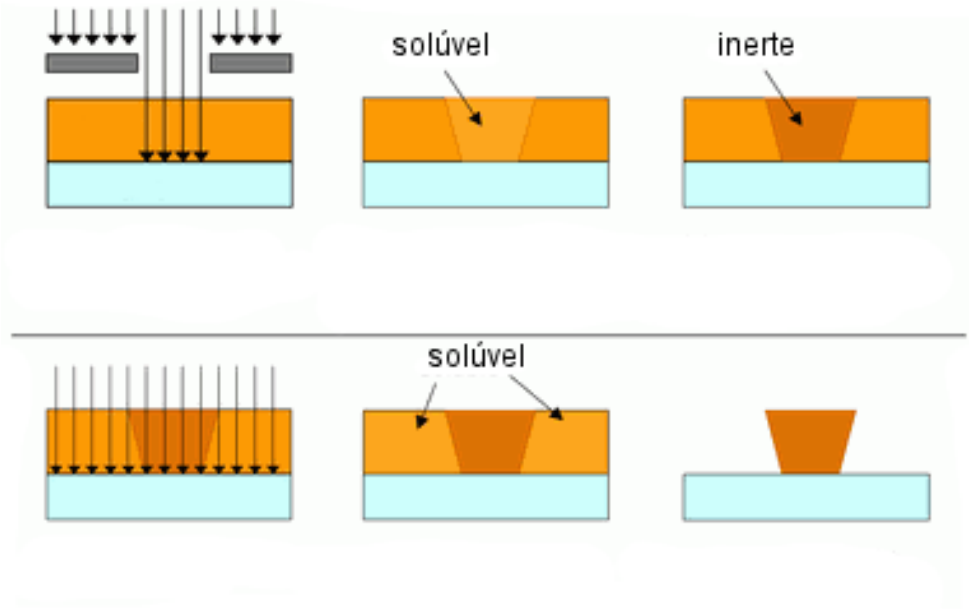

Fonte: adaptado de MicroChemicals (2012)

exposição em todo filme, a região não exposta na primeira etapa torna-se solúvel para a revelação (KOCH; RINKE, 2017).

1.3.2 Fabricação de filmes finos

Neste estudo, foram fabricados filmes finos por diferentes técnicas—a deposição física por vapor assistida por feixe de elétrons (*electron-beam PVD*) (EBPVD) para filmes metálicos; deposição por camadas atômicas (*Atomic Layer Deposition*) (ALD) para Al_2O_3, e deposição física por vapor (PVD) simples para moléculas orgânicas (FRANSSILA, 2010).

2 OBJETIVOS

Produzir transistores orgânicos de filmes finos ultracompactos, flexíveis e de baixa tensão de operação através da utilização de nanomembranas autoenroladas.

Para tanto, este estudo teve como objetivos específicos:

- Fabricar os dispositivos em configuração tubular através da técnica de autoenrolamento baseado em nanomembranas tensionadas.
- Comparar características elétricas e estruturais entre as arquiteturas tubular e planar entre si e com a literatura.
- Demonstrar o funcionamento dos dispositivos com aplicações em circuitos simples.

3 ARTIGO ORIGINADOS DO TRABALHO

O artigo a seguir foi publicado em Nano Letters 2018, 18, 5552–5561
DOI: 10.1021/acs.nanolett.8b01958

As figuras 5–16 são de própria autoria e elaboradas em 2018.

3.1 Low-Voltage, Flexible, and Self-Encapsulated Ultracompact Organic Thin-Film Transistors Based on Nanomembranes

Kleyton Torikai[†‡], Rafael Furlan de Oliveira[†] , Davi H. Starnini de Camargo[†‡], and Carlos C. Bof Bufon*[†‡]

[†] Brazilian Nanotechnology National Laboratory (LNNano), Brazilian Center for Research in Energy and Materials (CNPEM), Campinas, 13083-970 São Paulo, Brazil

[‡] Postgraduate Program in Materials Science and Technology (POSMAT), São Paulo State University (UNESP), Bauru, 17033-360 São Paulo, Brazil

3.1.1 Abstract

Organic thin-film transistors (OTFTs) are an ever-growing subject of research, powering recent technologies such as flexible and wearable electronics. Currently, many studies are being carried out to push forward the state-of-the-art OTFT technology to achieve characteristics that include high carrier mobility, low power consumption, flexibility, and the ability to operate under harsh conditions. Here, we tackle this task by proposing a novel OTFT architecture exploring the so-called rolled-up nanomembrane technology to fabricate low-voltage (<2 V), ultracompact OTFTs. As the OTFT gate electrode, we use strained nanomembranes, which allows all transistor components to be rolled-up and confined into a tubular-shaped tridimensional device structure with reduced footprint (ca. 90% of their planar counterpart), without any loss of electrical performance. Such an innovative architecture endows the OTFTs high mechanical flexibility (bending radius of <30 μm) and robustness—the devices can be reversibly deformed, withstanding more than 500 radial compression/decompression cycles. Additionally, the tubular device design possesses an inherent self-encapsulation characteristic that protects the OTFT active region from degradation by UV-light and hazardous vapors. The reported strategy is also shown to be compatible with different organic semiconductor materials. All of these characteristics contribute to further extending the potentialities of OTFTs, mainly toward rugged electronics.

Keywords: flexible electronics; organic thin-film transistors (OTFTs); rugged electronics; strained nanomembranes; ultracompact devices;

Figura 4 – Graphical abstract

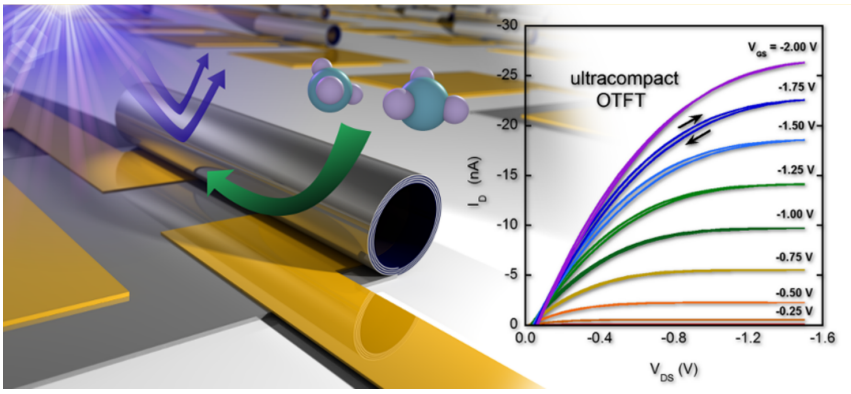

3.1.2 Main text

Over the past two decades, research has made evident the technological potential of organic thin-film transistors (OTFTs) for future electronics. The main envisioned OTFT applications are those that cannot be fulfilled by inorganic devices (SIRRINGHAUS, 2014; HOROWITZ, 1998; SHULAKER et al., 2017; HAN et al., 2017; NIKOLKA et al., 2017), for example, in large-area and flexible electronics, such as bendable/stretchable displays (LEYDECKER et al., 2016; OH et al., 2016; CHOI; KIM; HA, 2008; DIMITRAKOPOULOS; MALENFANT, 2002; NOMURA et al., 2004; PARK et al., 2014). The OTFT applications are intended to benefit from the intrinsic characteristics of organic semiconductors (OSCs), such as mechanical flexibility, low-temperature processing, and high-throughput manufacturing at low costs (e.g., from printing) (FORREST, 2004). Additional device characteristics, viz., low-voltage operation, effective signal amplification ability, ease of miniaturization/integration, and biocompatibility, are desirable in OTFTs and have been pursued for several innovative applications. These include consumer electronics, i.e., smart home and personal devices, and solutions for the automotive and medical industries, such as sensors and biosensors (GUO et al., 2017; SOMEYA; BAO; MALLIARAS, 2016). Finally, the possibility to boost and tailor the OSC properties, through chemical synthesis, allows the continuous development of devices with novel functionalities and improved performance (FACCHETTI, 2007; HENSON; MÜLLEN; BAZAN, 2012; KUNUGI et al., 2003). All of these characteristics make the technological opportunities for OTFTs vast, exciting, and promising.

Recent discussions about the OTFT challenges to conceive such a variety of applications call attention mainly to the device manufacturing (GUO et al., 2017). Commercial applications demand large-scale production. Thus, it is highly desirable to get the OTFT

fabrication processes into existing manufacturing routes, e.g., through microfabrication processes from the semiconductor industry (GUO et al., 2017). Devices designed and produced using well-established methods can be better scaled, reproduced, and optimized by the interplay between manufacturing and performance, which is a leading concern in OTFT development (GUO et al., 2017). The manufacturing processes also impact stability, both storage and operational, another matter in this field with severe consequences to the final OTFT application. In this sense, several efforts have been made to address the performance/stability issues in OTFTs from the perspective of manufacturing (KIM et al., 2018). Despite the advances in this direction, a significant gap still exists between the current OTFT technology and the well-established inorganic semiconductors when it comes to rugged electronics. The main reason is that OSC-based devices are very susceptible to extreme conditions, e.g., mechanical stress, and exposure to gases and radiation (BASIRICÒ et al., 2017). Hence, the manufacturing needs to take into account the OTFT robustness to develop devices for more realistic applications. Finally, the use of standardized fabrication methods does not prevent OTFTs from being customized for specific usages, for example, by engineering the device architecture (DESBIEF et al., 2016). Such an approach is crucial as the current technology exhibits an ever-growing demand for complex functions to be performed by electronic devices, where innovative OTFT architectures will be necessary for the technological progress.

One method that can address most of the current requirements for OTFT technology—mainly those regarding batch processing and standardized fabrication, miniaturization, integration, and the addition of novel functionalities in a single platform—is the assembly of nanomembranes (NMs) (SCHMIDT; EBERL, 2001; MÜLLER et al., 2012). Nanomembranes are single or multilayered structures, micrometer-wide with a few nanometers thickness, able to stand freely in air or vacuum in a variety of forms (MATOVIC; JAKŠIĆ, 2009). Having high flexibility, due to their large aspect ratio, the NMs are very suitable for device fabrication, allowing the design of two-dimensional (2D) structures to evolve into tridimensional (3D) advanced structures (MATOVIC; JAKŠIĆ, 2009; FROETER et al., 2013; HUANG; MEI, 2012). Ultracompact capacitors (BUFON et al., 2010; SHARMA et al., 2014; DENG et al., 2016; WANG et al., 2016; PETRINI et al., 2018), micropumps (SOLOVEV et al., 2011a), micromachines (SOLOVEV et al., 2011b), optical microcavities (WANG et al., 2017), inductors (HUANG et al., 2012; YU et al., 2015), heterojunctions (BUFON et al., 2011; THURMER et al., 2010; BENDOVA et al., 2016; MERCES et al., 2017; OLIVEIRA et al., 2018), batteries (HUANG et al., 2017), sensors (MARTINEZ-CISNEROS et al., 2014; MÖNCH et al., 2011; VERVACKE et al., 2014), and even an inorganic field-effect transistor (GRIMM et al., 2013) are some successful examples on the use of the NM technology for device development. The resulting applications directly benefit from the NM characteristics; e.g., the ultracompactness and sizable active area are suitable for energy storage elements, while mechanical robustness and softness are desirable

for the establishment of electrical connections with molecular materials. Therefore, the versatility of NMs can be advantageous to develop OTFTs with improved characteristics, meeting several demands of the current technology.

In the following, we report on the manufacturing of 3D, ultracompact OTFTs that present remarkable flexibility, mechanical robustness, self-encapsulation characteristics, and low-voltage operation (<2 V), via NM engineering. The so-called rolled-up OTFTs (r-OTFTs) are attained by fabricating planar bottom-gate bottom-contact OTFTs that are reshaped into cylindrical devices without compromising the electrical performance. The entire device manufacturing is based on standard microfabrication processes, viz., optical lithography and thin-film deposition methods. The planar transistors (p-OTFTs), assembled onto a host substrate, curl-up after the selective removal of a GeO_x sacrificial layer positioned underneath the devices—a consolidated strategy for the fabrication of several inorganic NM-based applications (BUFON et al., 2010; SHARMA et al., 2014). The r-OTFT exhibits a reduced footprint area, air-stability, low-voltage operation (<2 V), high flexibility (bending radius <30 μm), mechanical robustness (viz., endurance of several compression and decompression cycles), and a self-protective structure toward the exposure to UV-light and ammonia vapor. All of these characteristics endow the r-OTFTs with potentialities to be exploited in a multitude of applications, from aerospace technology to smart circuitry for agriculture.

The fabrication of r-OTFTs is based on the spontaneous roll-up of planar organic transistors (p-OTFTs) assembled onto GeO_x-coated glass substrates. The selective removal of the GeO_x sacrificial layer allows the deterministic release of the NM's stored elastic energy, curling-up the planar structures into 3D cylindrical-shaped devices. The layout and layer components of both p- and r-OTFT geometries are shown in Figura 5.

A thin NM, made of a bimetallic layer of Ti/Cr (15 nm/20 nm), which is used to create the strain to roll-up the p-OTFTs, also acts as the transistor gate electrode. As the gate dielectric, we employed a thin (20 nm) Al_2O_3 film grown by atomic layer deposition (ALD), further coated with a self-assembled monolayer (SAM) of octadecylphosphonic acid (ODPA). The use of ODPA-SAM has been reported as strategic for the functionalization of the gate dielectric to improve the OTFT performance (SU et al., 2013). The OTFT channel region was defined using interdigitated Au/Cr source (S) and drain (D) electrodes with a width/length (W/L) ratio of 153. The SD electrodes (10 nm thick) were patterned onto the gate dielectric before the ODPA-SAM functionalization. As the OSC material, we employed copper(II) phthalocyanine (CuPc) thin-films (20 nm) that possess broad applicability in OTFTs (MELVILLE; LESSARD; BENDER, 2015) and the reported stability in water (OLIVEIRA et al., 2016) necessary for the dissolution of GeO_x during the roll-up procedure. Furthermore, CuPc is also extensively used in optoelectronics due to its absorption spectra in the UV–vis region (FARAG, 2007), making it a suitable material to study the effects of light exposure on the OTFT performance. The device structure also

Figura 5 – OTFT layout and layer composition.

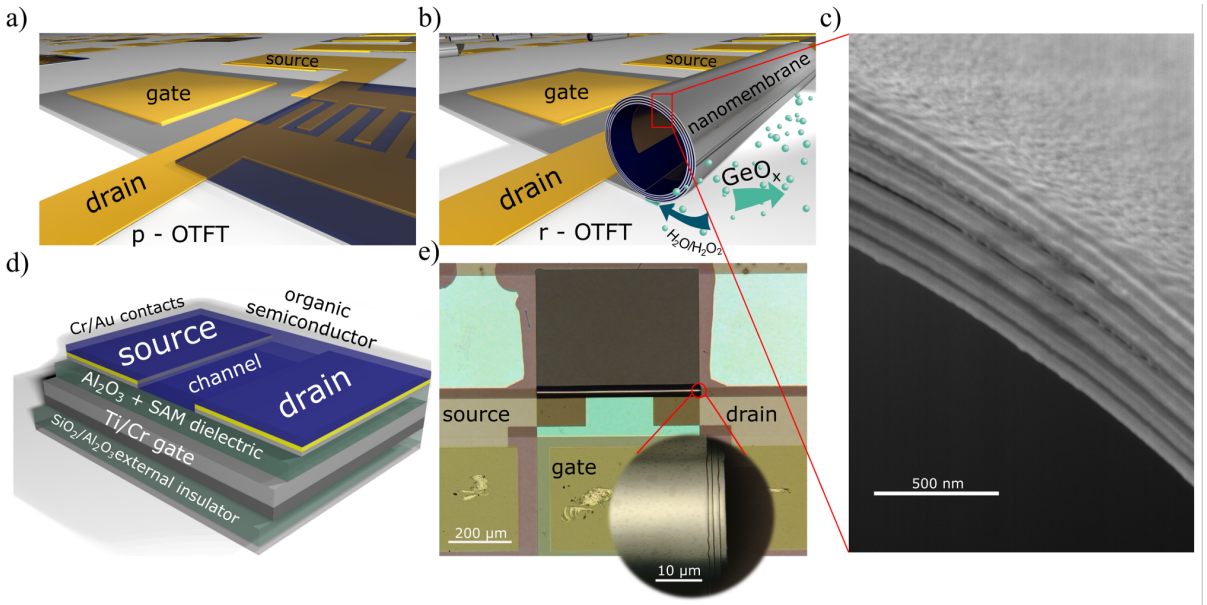

Tridimensional layout of (a) planar (p-OTFTs) and (b) rolled-up (r-OTFTs) devices, illustrating the dissolution of GeO_x sacrificial layer. (c) Scanning electron microscopy (SEM) image of the r-OTFT cross-section showing the device layers (five windings) closely packed. The sample was prepared by focused ion beam (FIB). (d) OTFT layer schematics. (e) Optical confocal microscopy image of an r-OTFT (inset for details), indicating the source, drain, and gate terminals. The average r-OTFT external radius is ca. 14–30 μm.

contains a thin (10 nm/20 nm) SiO_2/Al_2O_3 external bilayer to insulate successive windings of the r-OTFTs electrically. Finally, the dissolution of GeO_x takes place by immersing the p-OTFTs in a 1% H_2O_2 (v/v) aqueous solution. The resulting r-OTFTs presented an average of five windings, with an external radius of ca. 14–30 μm, length of ~370 μm, and a lateral dimension of 500 μm. Additional details about the device fabrication are presented in the Experimental Section.

To validate the strategy for the production of ultracompact r-OTFTs from planar organic transistors, we evaluated and compared the electrical response of both device architectures. Figura 6 shows the respective output (I_D versus V_{DS}) and the transfer (I_D and $\sqrt{I_D}$ versus V_{GS}) characteristics of both p- and r-OTFTs. All measurements were performed at room temperature in laboratory atmosphere.

The typical p-type behavior reported for CuPc OTFTs (MELVILLE; LESSARD; BENDER, 2015) is observed here for p- and r-OTFTs at low operational voltages (<2 V). Both types of devices exhibited well-defined linear and saturation regimes (Figura 6c,d). The observed lower back sweep current (BSC) hysteresis is often attributed to charge carrier trapping at the channel interface (EGGINGER et al., 2009). Here, BSC hysteresis is considerably small and equally present for both OTFT architectures and, therefore, can be neglected for their comparison. Gate leakage currents (I_G) lower than 1 nA were

Figura 6 – Electrical response of CuPc p-OTFTs and r-OTFTs.

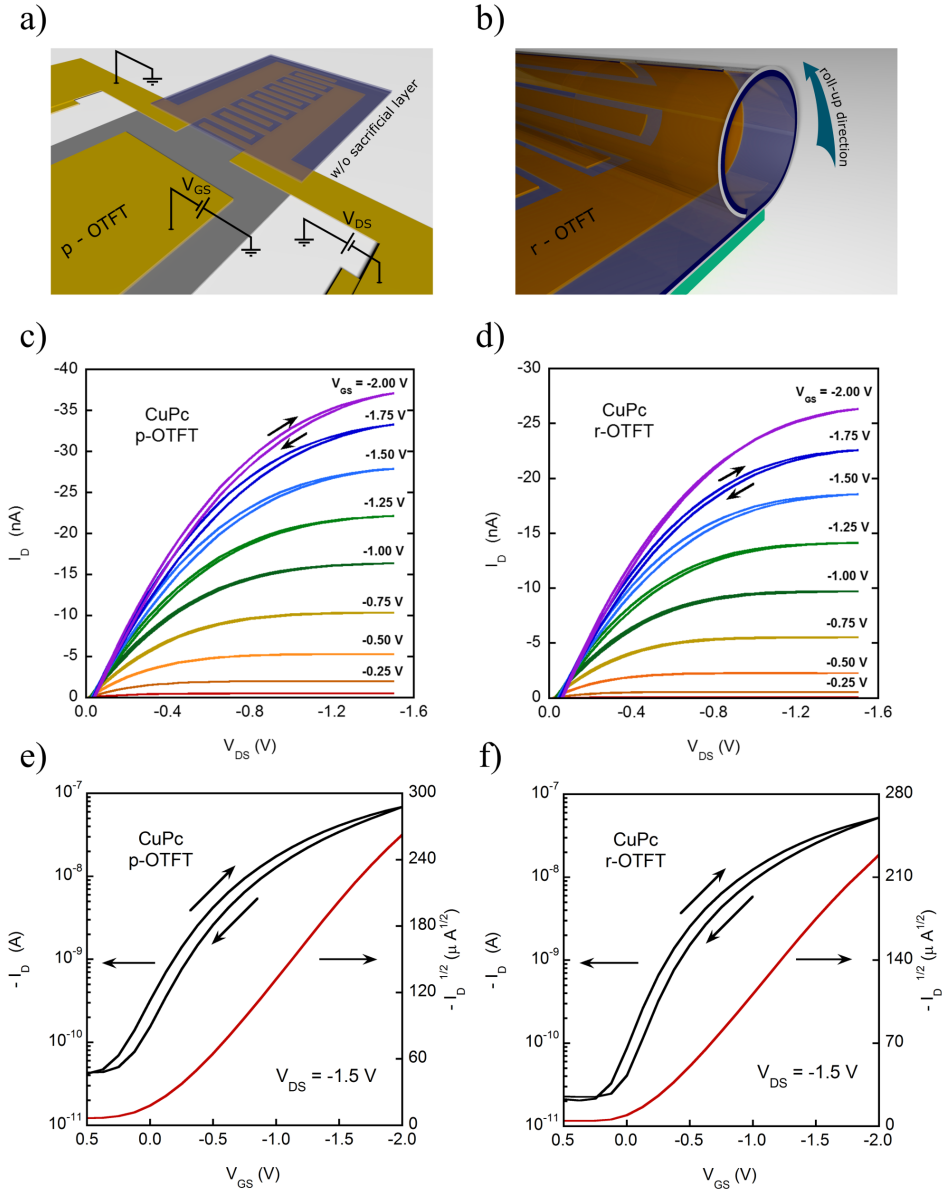

(a, b) Schematics of p- and r-OTFT architectures. (c, d) Respective transistor output curves and (e, f) transfer characteristics in the saturation regime ($V_{DS} = -1.5$ V). The measurements were carried out at room temperature in a laboratory atmosphere. The arrows indicate the hysteresis direction.

obtained for both types of devices, in agreement with other low-voltage OTFTs comprising a thin Al_2O_3 gate dielectric (URASINSKA-WOJCIK et al., 2015). The respective gate leakage curves of p- and r-OTFTs are shown in the Supporting Information (SI, Figura 10). The comparison between the electrical characteristics of p-OTFTs and r-OTFTs indicates minor differences. From Figura 6e,f, one can observe slightly lower I_D and higher I_{OFF} for the CuPc r-OTFT, in respect to the planar transistor. Such small differences, however, are not sufficient to note significant changes, for example, in the device I_{ON}/I_{OFF} ratio. Here, we find I_{ON}/I_{OFF} of $\sim 10^3$ for both OTFT architectures. The subthreshold swing (SS) for

both p- and r-OTFTs is in the range 359–430 mV dec^{-1}. The transconductances (g_m) are also similar, having measured values found in the 61–83 nS range. From the square-root of I_D in the saturation regime (Figura 6e,f, red curve), the OSC charge carrier mobility (μ) and the device threshold voltage (V_{TH}) have been calculated using the following equation:

$$I_D = \frac{W}{2L}\mu C_I \left(V_{GS} - V_{TH}\right)^2 \qquad V_{DS} > \left(V_{GS} - V_{TH}\right) \tag{3.1}$$

where W and L stand, respectively, for the width and length of the OTFT channel region. C_I is the insulator specific capacitance (∼200 nF cm^{-2}), which was determined using the dielectric constants and thicknesses of both the ODPA-SAM and the Al_2O_3 gate dielectric layers (see the SI for details). From Figura 6e,f and using eq (3.1), we find $\mu = (1.1 \pm 0.1) \times 10^{-3}$ cm^2 V^{-1} s^{-1} and $V_{TH} = 0.26 \pm 0.04$ V for p-OTFTs, and $\mu = (1.3 \pm 0.1) \times 10^{-3}$ cm^2 V^{-1} s^{-1} and $V_{TH} = 0.09 \pm 0.13$ V for r-OTFTs. The calculated μ values are similar to each other and agree with values found in the literature for other CuPc OTFTs (SU et al., 2013; BAO; LOVINGER; DODABALAPUR, 1996; NÉNON et al., 2010; SUBBARAO et al., 2016). Higher μ, however, can be achieved using a different OSC, as the method is compatible with water-stable materials (details discussed hereafter).

In contrast to the carrier mobility, V_{TH} presented a considerable divergence regarding the two OTFT architectures. V_{TH} fluctuations have been recently reported for water-gated CuPc transistors (OLIVEIRA et al., 2016). In this case, ions in solution diffuse into the CuPc film structure causing variations of V_{TH} in the mV range. Such water-related effects can also be ascribed as the source of the observed V_{TH} fluctuations. Here, both p- and r-OTFTs were fabricated on the same chip and, therefore, were exposed to the very same procedures and conditions (viz., low-concentration H_2O_2/H_2O solution to carry out the roll-up processes). The difference, however, lies in the absence of the GeO_x sacrificial layer underneath the p-OTFTs, preventing them from curling-up. Thus, the water uptake is likely to be different considering the device architectures. Nonetheless, CuPc thin-films can be referred to as water-stable as their semiconducting properties are preserved after water exposure (SOMEYA; BAO; MALLIARAS, 2016; OLIVEIRA et al., 2016).

Despite the small differences found in the operation of planar and tubular devices, their similar responses indicate that the roll-up process does not lead to appreciable loss of electrical performance. Such a conclusion is further corroborated by the response of p- and r-OTFTs employing another OSC material, namely, dinaphtho[2,3-*b*:2′,3′-*f*]thieno[3,2-*b*]thiophene (DNTT), as discussed hereafter. The fabrication of 3D, tubular-shaped OTFTs with no loss of performance is a remarkable achievement considering the substantial device downscaling (reduction of ca. 90% in the area occupied in the planar configuration). The 90% reduction represents a significant device miniaturization, which is extremely important for the development of compact electronics. Also, the miniaturization is further facilitated by employing standardized device fabrication techniques, which is crucial for producing more complex device arrangements, for example, unipolar inverters (Figura 11).

The use of NMs and, consequently, the roll-up process endows the tubular OTFTs two additional characteristics that are very attractive for modern electronics, namely, flexibility and mechanical robustness. To assess such characteristics, we monitored the response of CuPc r-OTFTs under static and dynamic mechanical stress. A rounded tip compressed the r-OTFTs to bend the tubular structure inward in the radial direction (Figura 7a). For a static stimulus, we recorded the transfer characteristics of r-OTFTs in the saturation regime ($V_{DS} = -1.5$ V) while pressing them vertically until the inner device walls were closer than the initial tube radius. The resulting electrical response was compared to the transfer curves obtained before the application of the mechanical stimulus, and immediately after its release (Figura 7b). An image of the r-OTFT under static compression is shown in Figura 12. Finally, the response of r-OTFTs was also investigated under an intermittent mechanical stimulus using a calibrated piezoelectric actuator. In this case, changes in the r-OTFT current in the saturation regime ($V_{DS} = -1.5$ V and $V_{GS} = -2.0$ V) were monitored for compression/decompression cycles at two frequencies, viz., 0.1 and 0.5 Hz (Figura 7c–e). A video showing the intermittent compression of the r-OTFTs while recording the electrical response is presented as Video S1, Supporting Information. Additional experimental details about the assessment of the r-OTFT mechanical properties are given in the Experimental Section.

The r-OTFTs have been shown to be both highly flexible and mechanically robust. After full compression of the devices, the tubular structure returns to its original shape as the mechanical stress is released. No damage is observed in r-OTFTs after removing the mechanical stimulus. From Figura 7b, we find that the r-OTFT transfer curves overlap for electrical measurements taken before the mechanical stimulation, during the full tube compression, and after the stress release. Some device parameters such as μ, g_m, and the I_{ON}/I_{OFF} ratio are also not significantly altered (Tabela 1). The conservation of the r-OTFT leakage currents after the mechanical compression also corroborates the r-OTFT mechanical robustness (Figura 13). Minor changes of I_D, however, occur because of the mechanical compression, as visualized during an intermittent mechanical stimulus (Figura 7e). Figura 7d shows the voltage signal of the piezoelectric actuator responsible for the tube mechanical stimulation at 0.1 and 0.5 Hz. Negative voltages correspond to the compressive movement, where -1 V refers to maximum tube compression (inner tube walls closer than the initial radius). The positive voltage bias is related to the tube decompression, where $+1$ V applies to the stress-free situation. The respective response of CuPc r-OTFTs under the intermittent mechanical stimulus is shown in Figura 7e. The r-OTFT electrical response has proven to be capable of following the mechanical oscillations, with no apparent delays. Current changes of about 0.3% have been recorded at the two referred frequencies. The r-OTFTs endured ca. 500 compression/decompression cycles of mechanical stress without presenting either significant mechanical or electrical failure. Nonetheless, higher mechanical oscillation frequencies or a greater number of

Figura 7 – Mechanical properties of r-OTFTs.

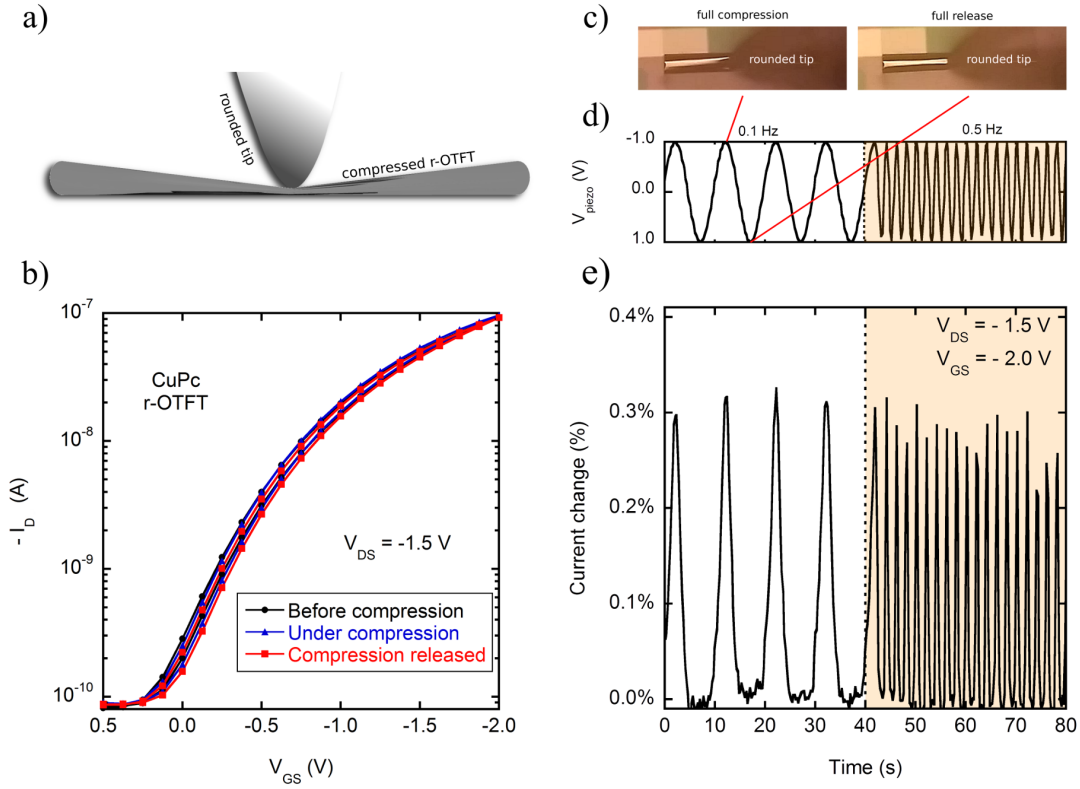

(a) Schematics (lateral view) of the CuPc r-OTFT during the application of a vertical compression by a rounded tip. (b) Transfer characteristics in the saturation regime ($V_{DS} = -1.5$ V) for the CuPc r-OTFT before, under, and after static compression (reverse voltage sweep). (c) Images of the r-OTFT under full compression (left) and release (right) during the intermittent mechanical stimulus. (d) Voltage signal of the piezoelectric actuator during the intermittent mechanical stimulus at the frequencies 0.1 and 0.5 Hz. Negative voltages indicate compression while the positive ones refer to the tip retreat. (e) Respective current changes (in percentage) acquired in the saturation regime ($V_{DS} = -1.5$ V and $V_{GS} = -2.0$ V) for the CuPc r-OTFT under the intermittent mechanical stimulus. The measurements were carried out at room temperature in a laboratory atmosphere.

compression/decompression cycles disrupt the r-OTFT operation. In spite of that, we attribute the observed superior flexibility and resilience of r-OTFTs to the intrinsic mechanical properties of NMs (MATOVIC; JAKŠIĆ, 2009), resulting in an innovative OTFT architecture. Such a performance is remarkable as one of the most frequent reasons for reliability degradation in flexible OTFTs is the strain-induced damage caused by mechanical conformation (SEKITANI et al., 2010).

In addition to mechanical stress, light irradiation and gas exposure are well-known sources of degradation for OTFT performance (SATO et al., 2016; SCHOLZ et al., 2015). Here, as the r-OTFT active area is enclosed within the tubular structure—with part of the channel embedded in between successive tube windings—an inherent self-protective characteristic toward such external agents is expected. To evaluate such features, we investigated the effects of UV-light and ammonia (NH_3) exposure on the electrical response

of both p- and r-OTFTs. For the transistor illumination, unfiltered UV radiation was provided at doses of 200 mJ cm^{-2}. The transfer characteristics in the saturation regime of both devices were recorded after each radiation dose. The carrier mobility for each transistor architecture was monitored during cumulative exposures (Figura 8a,c). To test the device self-encapsulation characteristics toward vapor exposure, we subjected p- and r-OTFTs to an ammonia-saturated atmosphere. The electrical responses of the respective devices were recorded after 5 min of conditioning in the NH_3 atmosphere, while the postexposure measurements were taken after venting the system for 1 h with air (2 bar). The data were compared with the p- and r-OTFT response in the pre-exposure condition (Figura 8b,d). Additional details about the UV-light and NH_3 exposure are presented in the Experimental Section.

Figura 8 – Evaluation of the r-OTFT self-encapsulation characteristics.

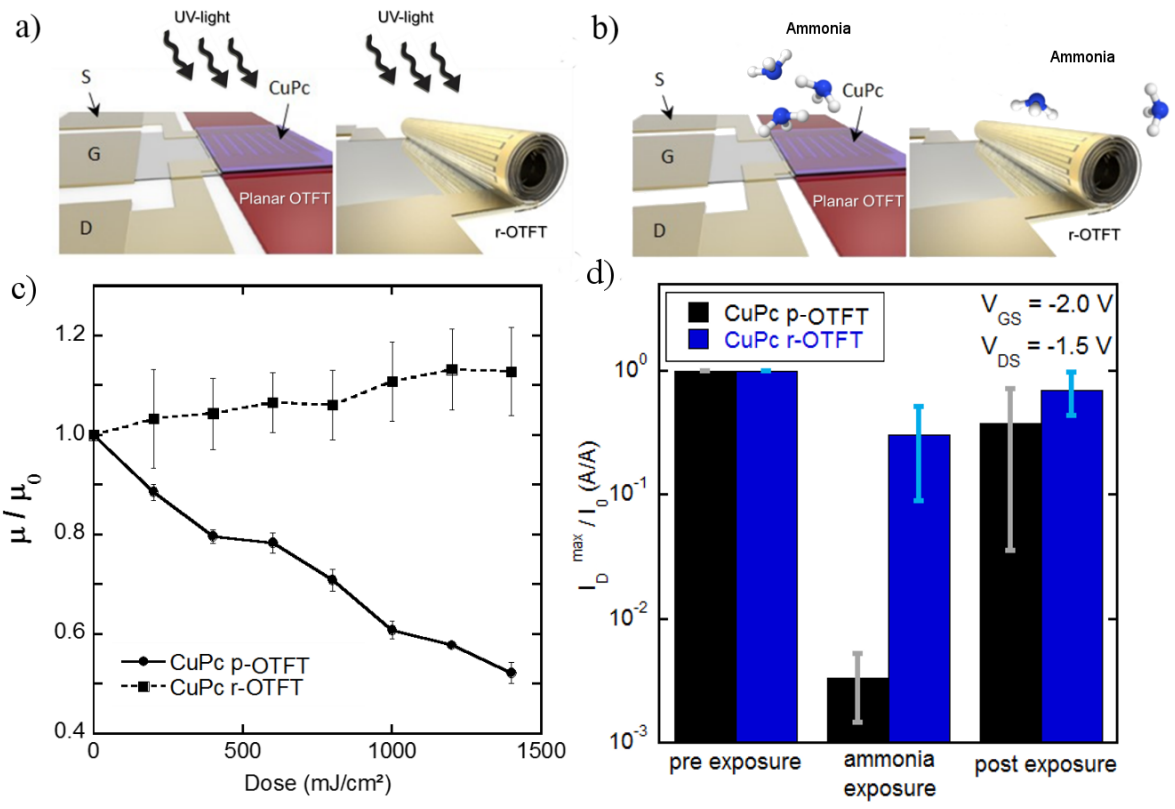

(a, b) Schematics of p- and r-OTFT devices exposed to UV light and ammonia-saturated atmosphere, respectively. (c) Normalized charge carrier mobility (μ/μ_0, saturation regime) versus the UV-light dose for illuminated p- and r-OTFTs. (d) Normalized maximum drain current ($I_D{}^{max}/I_0$) before, during, and after exposure to the ammonia-saturated atmosphere. For both experiments, the error bars correspond to deviations on the response of three similar devices.

The CuPc thin-films are reported to be good absorbers of UV–vis radiation, with a broad absorption band in the UV region (from 210 to <385 nm). Such an absorption range is related to transitions of π electrons to the partially occupied d metal orbitals.

The CuPc *Q*-bands, due to π–π^* transitions, occur at the visible region (viz., 550–750 nm) (FARAG, 2007). The UV absorption band of CuPc thin-films overlaps the spectral emission lines of the UV-light source used here (Figura 14). Thus, one may expect some photoresponse from the CuPc OTFTs due to UV irradiation. Some contribution in the visible range (viz., 550–600 nm) also cannot be disregarded (Figura 14). From Figura 8c, one can observe that the carrier mobility of illuminated p-OTFTs decreases substantially, reaching ca. 50% loss of its initial value (μ_0) for the maximum radiation dose used (1400 mJ cm^{-2}), while for r-OTFTs μ has varied slightly. In both cases, the observed changes of μ are progressive with the accumulative light dose.

The illumination of OSCs is known to generate three typical and different effects, namely, photoassisted oxidation, photoconduction, and photovoltaic behavior (DING et al., 2014; WATSON et al., 2018). Among these, photo-oxidation has been reported to cause a significant decrease of μ, ascribed to the reduction in the conjugation length of OSC molecules (FICKER et al., 2004). Photoconduction leads to an immediate current increase due to photogeneration of extra charge carriers. In the photovoltaic effect, a portion of photogenerated carriers may become trapped near to the OSC/dielectric interface, or in the dielectric itself (WATSON et al., 2018), leading to shifts of V_{TH} and, consequently, to changes in the OTFT transfer characteristics. Photo-oxidation cannot be ruled out to explain the substantial decrease of μ in the p-OTFTs since the channel is completely exposed to the radiation, oxygen, and atmospheric moisture. Conversely, in r-OTFTs, a significant fraction of the channel is embedded in between the device windings, thus preventing easy access of light and oxygen to the CuPc layer. Furthermore, the penetration depth of the UV radiation in the NM is considerably small (typically 10 nm). Therefore, the external coating of r-OTFTs prevents much of the UV radiation from going through the device and reaching the embedded OSC (estimated maximum transmittance of 3.5%, see the SI). The substantial μ decrease in p-OTFTs may have contributions from nonpermanent oxidative effects as well, such as the interfacial traps, as a partial recovery of μ (about 35%) has been observed after 18 h for devices stored in the air.

A similar rationalization used to explain the self-protective characteristics of r-OTFTs toward light irradiation applies to devices exposed to the ammonia-saturated atmosphere. In this case, as the transfer characteristics of NH_3-exposed transistors are severely affected, especially in p-OTFTs, we present the maximum I_{D} of the respective devices normalized by their initial current (I_0). Figura 8d shows a substantial decrease in max I_{D} for p-OTFTs, while the response of r-OTFTs is less affected by the ammonia vapor. For planar devices, I_{D} reduces by more than 2 orders of magnitude, while for r-OTFTs the current decrease represents less than 50%. Consequently, the postexposure response of r-OTFTs is closer to the pre-exposure one, when compared with the p-OTFTs. The corresponding current decrease in NH_3-exposed OTFTs relies on the spontaneous adsorption of NH_3 molecules on the CuPc thin-film surface, reducing the channel conductivity (BAGGIO et al., 2017).

The underlying interaction mechanism is based on the coordination of NH_3 molecules with the phthalocyanine metal center (BAGGIO et al., 2017). The NH_3 molecules behave as a Lewis base, transferring electrons to CuPc, which will eventually trap the mobile holes in the OTFT channel. Here, while ammonia molecules have unobstructed access to the whole p-OTFT surface, in r-OTFTs the admittance of NH_3 has been limited to the tube lateral apertures, with a significant part of the channel protected in between the NM windings. Thus, as long as the surface of the OSC channel is not entirely exposed for NH_3 adsorption, the effect of ammonia on the OTFT performance will be mild and substantially reversible. The responses of both p- and r-OTFTs are considerably recovered (after venting the sample compartment) as the binding energy of NH_3 with CuPc is relatively weak ($<$30 kJ mol^{-1}) (BAGGIO et al., 2017).

The above-discussed examples illustrate the ability of r-OTFTs to operate in harsh environments as a result of the innovative device architecture. For example, from the r-OTFT shielding toward UV irradiation, aerospace applications (e.g., satellite components) can be envisioned. Because of the device self-protective characteristics to ammonia exposure, smart circuitry using r-OTFTs for agricultural and environmental purposes is a possibility. The main reason is that NH_3 is a health threat to humans and animals, emitted in livestock and poultry farms because of the decomposition of manure, and related to the production of some fertilizers (TIMMER; OLTHUIS; BERG, 2005). Such device self-protection demonstrated for NH_3 vapor can be extrapolated to other atmospheric hazards. Finally, improvements on the UV and NH_3 self-protective characteristics of r-OTFTs can be achieved by selecting a more resistant OSC material for the transistor channel.

The fabrication of ultracompact OTFTs is versatile, allowing the use of different OSCs. The only necessary characteristic for this purpose lies on the water- and air-stability of the OSC material. Thus, to validate our experimental platform, we have fabricated r-OTFTs using dinaphtho[2,3-*b*:2′,3′-*f*]thieno[3,2-*b*]thiophene (DNTT), a small-molecule OSC, widely used in OTFTs, that satisfies the conditions mentioned above (DING et al., 2014; ZA'ABA; MORRISON; TAYLOR, 2017). The DNTT r-OTFTs were fabricated following the same experimental protocols and materials of CuPc devices, except for the absence of the ODPA-SAM gate dielectric coating. Figura 9 exhibits the output and transfer characteristics of p- and r-OTFTs based on DNTT.

As observed for the CuPc devices, the DNTT transistors presented similar low-voltage operation ($<$2 V) with well-defined linear and saturation regimes. The more pronounced BSC hysteresis in comparison with the CuPc devices is related to the absence of a SAM-treated gate dielectric, which may lead to stronger charge trapping at the interface with the OSC (DING et al., 2014). This effect is also observed by the transfer curves of such devices (Figura 9c,d), which present two different slopes confirming the presence of shallow traps in the channel. The main result, however, refers to the viability of using a different

Figura 9 – Electrical characteristics of DNTT r-OTFTs.

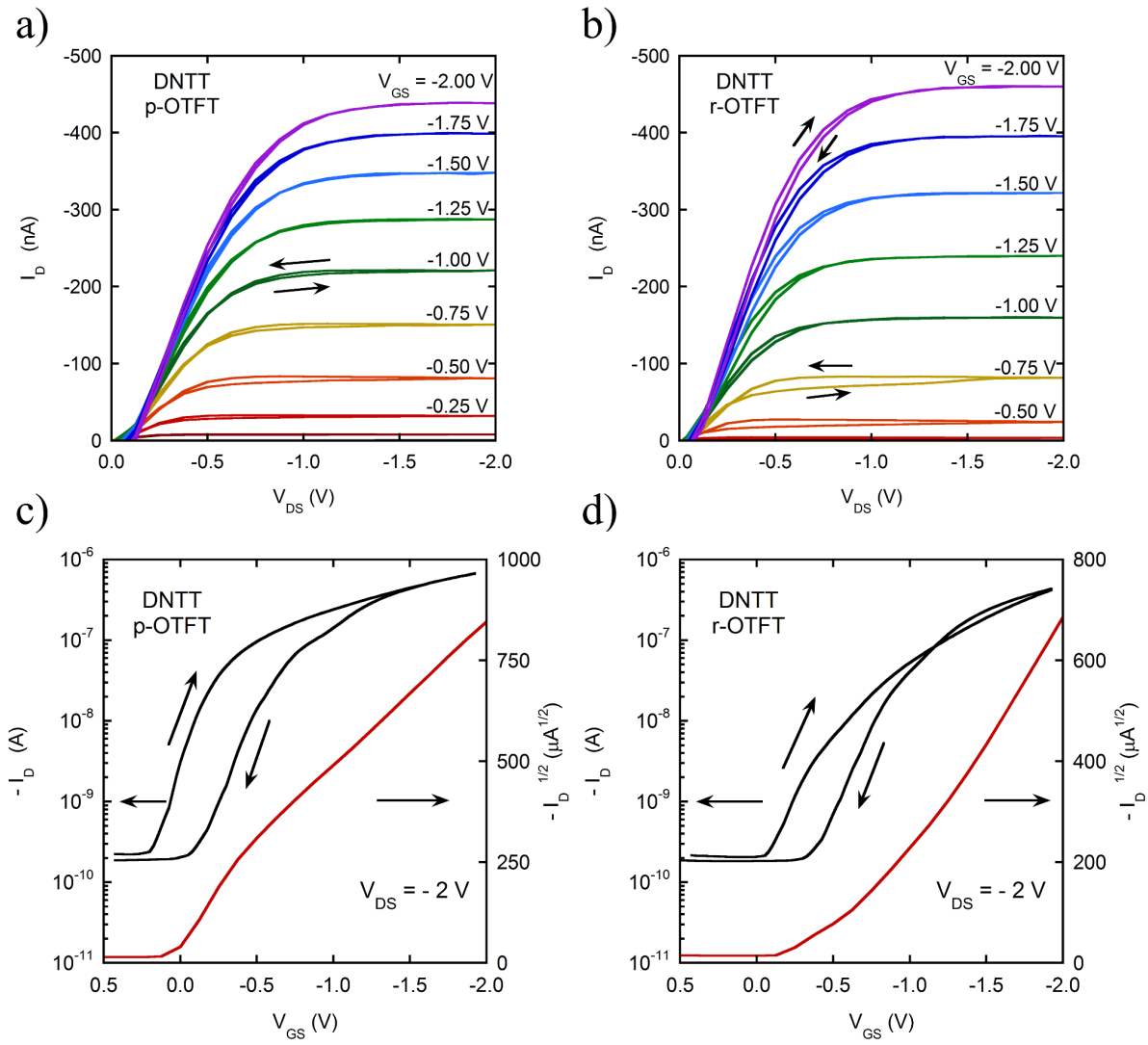

(a, b) Output and (c, d) transfer curves in the saturation regime ($V_{DS} = -1.5$ V) for planar and r-OTFTs based on DNTT. The measurements were carried out at room temperature in a laboratory atmosphere.

OSC material for the production of ultracompact r-OTFTs with no significant loss of performance, in comparison with their planar counterparts. Quantitative data regarding operational characteristics of DNTT p- and r-OTFTs are given in the SI (Tabela 2 and Figura 15). Our results demonstrate the versatility of the reported strategy to produce ultracompact OTFTs, expanding the methodology to other OSC materials.

In summary, we have shown that the rolled-up nanomembrane technology can be used to support innovative, tridimensional, low-voltage flexible organic devices, namely, thin-film transistors (OTFTs), with interesting electric and mechanical properties. The nanomembrane-based technology allowed us to incorporate novel features to OTFTs, inherent to the device architecture, such as a self-protective ability toward degradation by UV-light and ammonia exposure. Using standard microfabrication processes, e.g., pho-

tolithography and thin-film deposition, we prepared bottom-gate bottom-contact OTFTs using copper phthalocyanine (CuPc) and dinaphtho[2,3-*b*:2′,3′-*f*]thieno[3,2-*b*]thiophene (DNTT) as the organic semiconductor layers. The planar transistors (p-OTFTs) are assembled on top of a strained nanomembrane that self-rolls, after the selective removal of a sacrificial layer, adopting a 3D ultracompact architecture (r-OTFTs). This methodology produces OTFTs with reduced length from approximately 370 to 30 μm, i.e., $\sim$90% of the reduction in size, without loss of the electrical performance. Such r-OTFTs are mechanically robust, withstanding over 500 cycles of compression/decompression applied inward of the tube's radius, with inexpressive degradation. The ability to operate in harsh conditions, such as under UV-light and ammonia exposure or mechanical compression, shows the high resilience of r-OTFTs to different external factors that hinder the performance of conventional OTFTs. This differential demonstrates the potential of r-OTFTs for a multitude of applications, from aerospace technology to smart circuitry for agriculture, aiming for rugged organic electronics.

Experimental Section. Bottom-gate bottom-contact p- and r-OTFTs were fabricated on glass substrates subjected to an ultrasonic cleaning bath in VLSI acetone (40 min), further cleaned by piranha etching (5–10 min) and O_2 plasma (150 W, 18 s, 0.4 mbar). The germanium oxide sacrificial layer (GeO_x) is formed by depositing 20 nm of Ge by e-beam thermal evaporation at 1 Å s^{-1} that is further oxidized on a hot plate at 60 °C for 17 h. The OTFT external insulating layers were SiO_2 (10 nm), deposited by e-beam thermal evaporation (10^{-7} Torr, 1 Å s^{-1}, room temperature), and Al_2O_3 (20 nm) deposited by thermal ALD (Cambridge NanoTech Savannah 100 atomic layer deposition system) at 150 °C using trimethylaluminum (TMA) from Sigma-Aldrich and water as precursors. The Ti/Cr strained bilayer (15 nm/20 nm) was deposited by e-beam thermal evaporation at the rate of 3 and 7 Å s^{-1}, respectively. Here, the strained bilayer also acts as the transistor gate electrode. A 20 nm thick Al_2O_3 layer was used as the gate dielectric, and a 20 nm thick SiO_2 layer was used to suppress leakage current at the gate electrode edges, where the source and drain electrodes connect with their contact pads. Then, Cr/Au (5 nm/5 nm) source and drain contacts were fabricated by e-beam thermal evaporation (10^{-7} Torr, 1 Å s^{-1}, room temperature) and photolithography. Contact pads were deposited by first etching the Al_2O_3 layer on top of the gate contact with hydrogen fluoride (HF) aqueous solution (1% v/v) for 40 s, using photoresist AZ 5214E (Microchemicals) as a protective layer, followed by the deposition of Cr/Au (100 nm/400 nm) contact pads. The etching of the oxide layer was also carried out to create trenches for the dissolution of the GeO_x sacrificial layer during the roll-up process. A fraction of devices on the same chip were fabricated without the sacrificial layer, remaining in its planar configuration for comparisons. To terminate the gate dielectric composition, a SAM was applied on the Al_2O_3 by immersing the substrate in 2.5 mM ODPA solution prepared in isopropyl alcohol at 50 °C for 1 h, left to cool down at room temperature for 19 h. The devices

were then rinsed with warm and room-temperature isopropyl alcohol, and blow-dried with N_2. A 20 nm thick CuPc layer (powder, 576.08 g mol^{-1}, purchased from Alfa Aesar) was then thermally sublimated in a vacuum (10^{-6} Torr) at 3 Å s^{-1} deposition rate, with the substrate kept at room temperature to form the OTFT channel. Finally, for the roll-up procedure, the substrate was then immersed in 1% H_2O_2 (v/v) aqueous solution at 50 °C to remove the GeO_x sacrificial layer underneath the devices gradually. The whole roll-up process takes <3.5 h. Before the electrical measurements, the devices were kept for at least 2 h in a vacuum (10^{-2} Torr). The fabrication of DNTT transistors followed the same steps and conditions, except for the absence of the ODPA-SAM gate dielectric. DNTT (powder, 99%, 340.46 g mol^{-1}) was purchased from Sigma-Aldrich. All fabrication processes were carried out in a clean room environment, and the chemicals were used without further purification. The described device fabrication steps are illustrated in Figura 16 for clarity.

The p- and r-OTFTs were electrically characterized by measuring their output (I_D versus V_{DS}) and transfer (I_D and $\sqrt{I_D}$ versus V_{GS}) curves. The output curves were obtained by sweeping the drain-source voltage (V_{DS}) from 0 to −1.5 V at different gate-source biases (V_{GS}). The transfer characteristics were obtained at the saturation regime (V_{DS} = −1.5 V) varying V_{GS} from 0.5 to −2 V. All measurements were carried out in the ambient atmosphere using a Keithley 2636A SourceMeter unit. The devices were subjected to many measurement cycles until a stable response could be attained.

For an evaluation of the r-OTFT mechanical properties, static and intermittent compressions along the device radius were performed using a rounded copper tip controlled by a piezoelectric actuator (NanoCube XYZ Piezo Stage). The actuator was calibrated to provide full tube compression and complete release using a LVPZT controller and an FG100 function generator (digimess). Two compression frequencies have been tested, namely, 0.1 and 0.5 Hz. For the experiments related to the UV irradiation of p- and r-OTFTs, unfiltered UV light was provided by a mercury lamp (USHIO UV lamp USH-508S), with luminous flux 35200 lm, at cumulative doses of 200 mJ cm^{-2}. The electrical measurements were performed 5–10 min after the UV exposure, in an ambient atmosphere, to exclude the possibility of thermal-related effects to affect the device response. For experiments regarding vapor exposure, a chip containing p- and r-OTFTs was positioned into a small homemade compartment (∼50 cm^3), where the ammonia-saturated atmosphere was produced bubbling compressed air (2 bar) in a vial containing 5% v/v aqueous ammonia solution (∼28%, Sigma-Aldrich). In both experiments, with UV and NH_3 exposure, the OTFT electrical response was recorded using a Keithley 2636A SourceMeter unit at room temperature. Finally, device imaging has been performed using focused ion-beam-coupled scanning electron microscopy (FIB-SEM) in FEI Helios NanoLab 660 equipment, employing 2 kV acceleration and a through lens detector (TLD) in immersion mode. A Keyence VK-X200 3D laser scanning microscope was also used to image the devices.

3.1.3 Associated Content

Supporting Information

The Supporting Information is available free of charge on the ACS Publications website at DOI: 10.1021/acs.nano-lett.8b01958.

Additional figures including gate leakage curves, electrical responses, optical microscopy images, photograph, mercury lamp emission spectrum, and fabrication schematics (PDF)

Video S1: intermittent compression of the r-OTFTs while recording the electrical response (MPG)

3.1.4 Author Information

Corresponding Author

*E-mail: cesar.bof@lnnano.cnpem.br.

ORCID

Rafael Furlan de Oliveira: 0000-0001-8980-3587

Carlos C. Bof Bufon: 0000-0002-1493-8118

Author Contributions

K.T. fabricated the devices, and performed measurements and data interpretation. R.F.O. designed devices and experiments, and performed data interpretation. D.H.S.C. designed and fabricated devices. C.C.B.B. supervised the experiments and led the work. The manuscript was written through contributions of all authors. All authors have approved the final version of the manuscript.

Notes

The authors declare no competing financial interest.

3.1.5 Acknowledgments

This work was supported by CAPES, CNPq, and FAPESP (Project 2014/25979-2). We gratefully acknowledge D. M. Taylor (Bangor University/UK) for fruitful discussions, and L. D. Palermo and F. Montoro (LNNano/Brazil) for technical support.

3.1.6 Abbreviations

OTFT, organic thin-film transistor; OSC, organic semi-conductor; NM, nanomembrane; ALD, atomic layer deposition; ODPA-SAM, octadecylphosphonic acid self-assembled monolayer; CuPc, copper phthalocyanine; FIB-SEM, focused ion-beam scanning electron microscopy; BSC, back sweep current; DNTT, dinaphtho[2,3-*b*:2′,3′-*f*]thieno[3,2-*b*]thiophene.

Figura 10 – Gate leakage curves of CuPc OTFTs for both architectures.

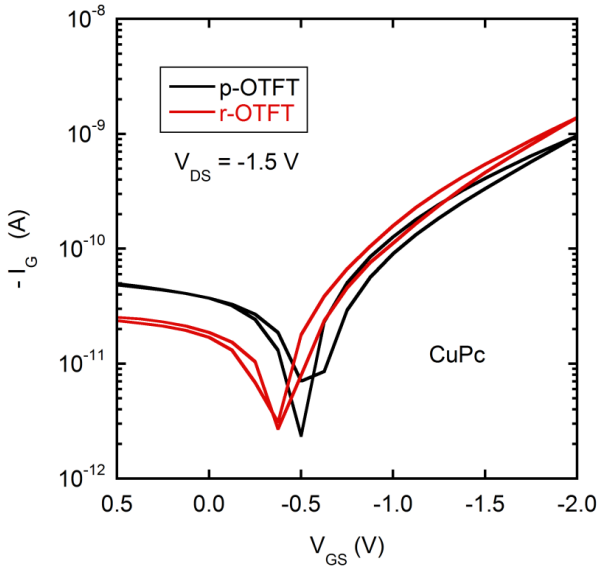

3.2 Supporting Information

Calculation of the dielectric specific capacitance (C_I)

The relative permittivity of the Al_2O_3 gate dielectric layer was obtained from the fabrication of several simple capacitors and measuring the capacitance at 1 kHz. The average value found is $\varepsilon_r = 5.6$. Assuming that the n-octadecylphosphonic acid self-assembled monolayer (ODPA-SAM) thickness is 2.1 nm and its relative permittivity (KLAUK et al., 2007) is 2.5, we calculate the specific capacitance:

$$C_\mathrm{total} = \left(\frac{1}{C_\mathrm{SAM}} + \frac{1}{C_{\mathrm{Al_2O_3}}} \right)^{-1} \cong 200\ \mathrm{nF\ cm^{-2}} \tag{3.2}$$

Unipolar inverters fabricated with r-OTFTs

One advantage on the use of standard microfabrication techniques for OTFT fabrication lies on the production of several devices on the same chip. Thus, a simple circuit application involving the connection of nearby OTFTs is the operation of unipolar inverters (BROWN et al., 1997). Here, we employed wire bonding technology for this purpose, although interconnects can be easily designed and assembled during the OTFT fabrication. Figura 11 shows the electrical characteristics of a unipolar p-type inverter formed by the association of two CuPc r-OTFTs.

From the inverter characteristics (Figura 11a), we observe an output signal compromised in ca. 8% for supply voltages (V_dd) of -1.0, -1.5, and -2.0 V. This may be a result of the gate leakage current experienced by the individual r-OTFTs or contact issues. Moreover, although a reasonable sharp switching is observed, considerable hysteresis in the inverter response is present. The observed hysteresis is also related with the inherent hysteresis

Figura 11 – Unipolar p-type inverter based on CuPc OTFTs.

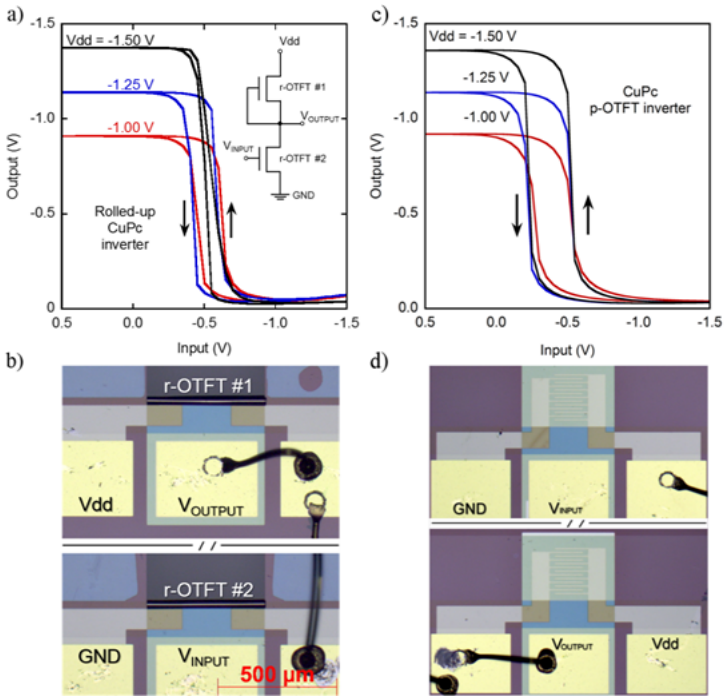

(a) Electrical response of r-OTFT unipolar inverter. Inset: respective unipolar inverter circuit. (b) Optical microscopy image showing the association of two CuPc r-OTFTs through wire bonding for the inverter operation. (c) Electrical response of p-OTFT inverter and its (d) respective microscopy image. The measurements were carried out at room temperature in laboratory atmosphere.

shown by the individual r-OTFTs in the main text (Figura 6f). The association of two hysteretic r-OTFTs worsens the inverter performance. For better inverter responses though, the electrical characteristics of the individual r-OTFTs have to be improved. Nevertheless, we emphasize the measured inverter characteristics are not inferior to those involving p-OTFTs (Figura 11c), which again corroborates the feasibility of our strategy for the fabrication of ultracompact organic devices.

Tabela 1 – CuPc r-OTFT electrical characteristics throughout mechanical stress.

	μ (10^{-3} cm^2/Vs)	V_{TH} (V)	ON/OFF ratio (A/A)	g_{m} (nS)
Before compression	1.5	0.04	$\propto 10^3$	86
Under compression	1.6	0.00	$\propto 10^3$	86
Compression released	1.6	−0.04	$\propto 10^3$	89

Estimated UV transmittance through r-OTFTs

In order to provide an upper limit to the transmittance of UV radiation through the nanomembrane (NM), we consider only the metallic strained bilayer (Ti/Cr in 15 nm/20 nm). Estimating the transmittance (T) considering internal transmission only, which follows Lambert's law:

$$T = e^{-\int_0^l \alpha(z)\mathrm{d}z} \tag{3.3}$$

Figura 12 – Static compression of the CuPc r-OTFT by a round needle tip.

Figura 13 – Gate leakage current during static mechanical compression.

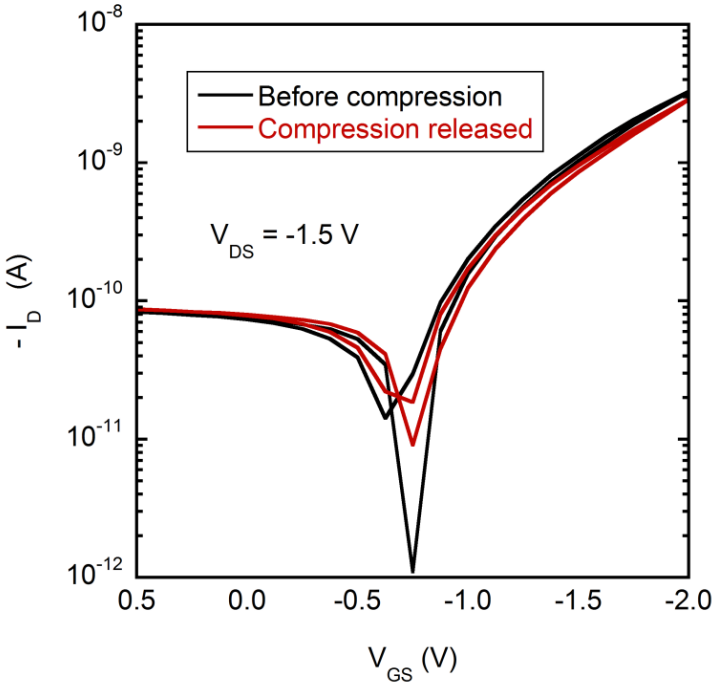

with l being the total thickness and $\alpha(z)$ the attenuation coefficient at depth z into the material. From the complex refractive index tables (JOHNSON; CHRISTY, 1974), the attenuation coefficient is obtained by:

$$\alpha = \frac{4\pi\kappa}{\lambda_0} \tag{3.4}$$

with λ_0 being the vacuum wavelength. For $\lambda_0 = 365$ nm, the calculated transmittance through the NM bilayer is $\sim$3.5%.

Figura 14 – Mercury lamp emission spectrum. Inset: absorption spectrum of CuPc thin-films adapted from Farag (2007).

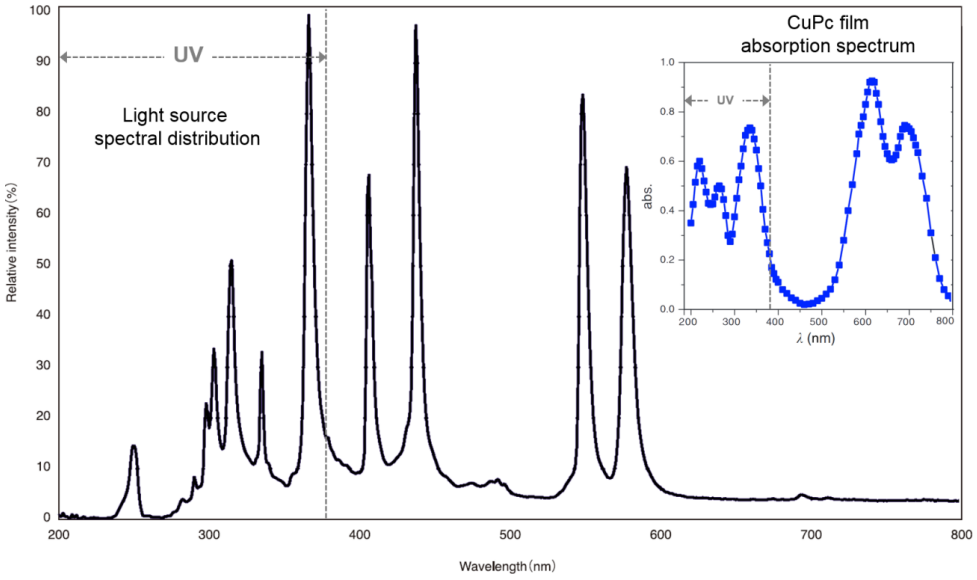

Tabela 2 – DNTT OTFTs electrical characteristics for both p- and r- architectures.

DNTT OTFT	μ (10^{-3} cm^2/Vs)	V_{TH} (V)	ON/OFF ratio (A/A)	g_{m} (nS)
p-	6.7	0.38	$\propto 10^3$	55
r-	13.5	-0.64	$\propto 10^3$	67

Figura 15 – Gate leakage curves of DNTT OTFTs for both architectures.

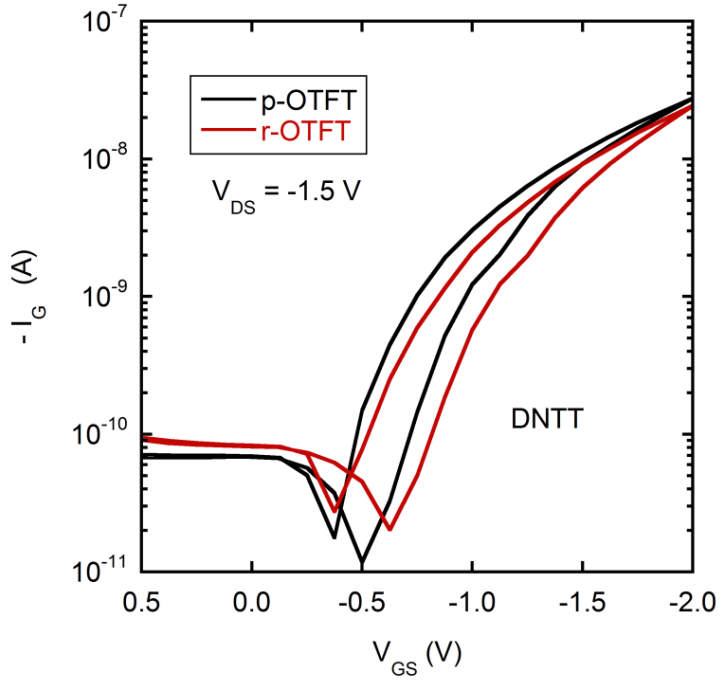

Figura 16 – Main step-by-step fabrication schematics.

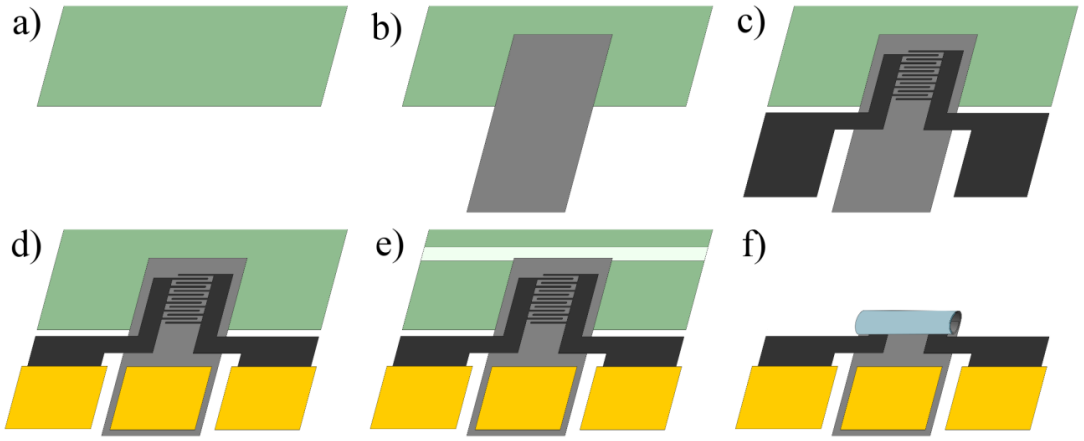

(a) GeO_x sacrificial layer followed by SiO_2 and Al_2O_3 external insulator. (b) Ti/Cr strained bi-layer and Al_2O_3 gate dielectric. (c) Cr/Au source and drain interdigitate electrodes. (d) Cr/Au contact pads. (e) Etching of oxide layers to allow H_2O_2 aqueous solution access to the sacrificial layer from the top of the device. (f) After the OSC deposition, removal of the sacrificial layer causes the device to roll-up in an ultra-compact tubular shape.

4 DISCUSSÃO

No artigo inserido na seção 3, discutem-se os experimentos e os resultados *finais* obtidos ao longo deste estudo. Para atingir estes resultados, houve um estudo extenso das mais diversas variáveis. Somente no processo de fabricação, temos:

- Deposições metálicas por EBPVD: Velocidades de deposição, espessuras de filme, intensidade e padrão do feixe de elétrons para cada material a ser depositado;
- ALD: fluxo do gás de arraste, durações e quantidade de pulsos dos precursores, temperatura de processo;
- Etching úmido: no caso de corrosão com ácido fluorídrico (HF), tempo de corrosão para cada espessura e concentração da solução;
- Deposição de moléculas orgânicas por evaporação: taxa de deposição e espessura para cada material utilizado;
- Autoenrolamento: concentração da solução para remoção da camada de sacrifício sem danificar o dispositivo, temperatura e tempo de processo.

Até que se obtivesse um conjunto de parâmetros apropriados que resultassem em dispositivos funcionais como ilustrados no artigo, foram realizados 5 lotes de fabricação, contando com 5 amostras por lote, em média. O tempo de fabricação de cada lote foi de 2–3 semanas em uma sala limpa. O resultado do autoenrolamento das NMs de uma amostra da segunda leva está ilustrado na Figura 17.

Figura 17 – Resultado de uma tentativa de autoenrolamento dos dispositivos de uma amostra do segundo lote de fabricação.

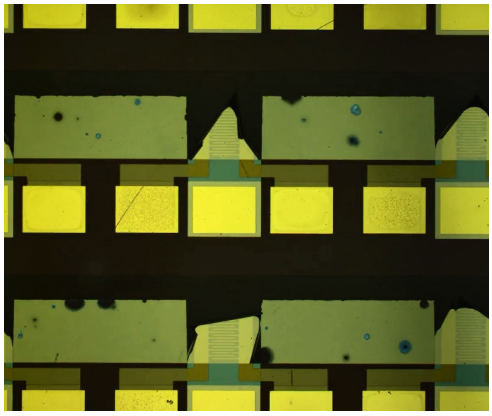

Fonte: o autor (2017)

Como pode-se inferir, se o processo de fabricação não é bem calibrado, a camada tensionada pode promover o autoenrolamento erraticamente—ou até mesmo romper-se.

4.1 Propriedades elétricas

A respeito da comparação do desempenho elétrico dos r-OTFTs fabricados com a literatura, pode-se observar que a mobilidade de portadores de carga obtida neste estudo está cerca de 2–3 ordens de grandeza abaixo do estado-da-arte (VIJAYAN et al., 2018; ZA'ABA; MORRISON; TAYLOR, 2017). Esta defasagem se dá por conta de diversos outros processos realizados sobre os OSCs—tratamento térmico, purificação, tratamento dos contatos elétricos, otimização da geometria—sendo que o desempenho elétrico não foi o foco deste trabalho. Os resultados obtidos estão condizentes com trabalhos que apresentam dispositivos similares, com o maior resultado sendo que o processo de autoenrolamento não prejudica o desempenho elétrico.

Estudos posteriores podem ser realizados no sentido de estender a lista de OSCs testados nesta nova arquitetura de dispositivo, assim expandindo a gama de possíveis aplicações. Em princípio, as condições necessárias para a fabricação nesta plataforma conforme descrita neste estudo são a resistência à atmosfera e à umidade.

4.2 Propriedades mecânicas

Como discutido no artigo, muitos dos defeitos em dispositivos baseados em OSCs são causados por estresse mecânico (SEKITANI et al., 2010). O resultado obtido é bastante supreendente neste sentido. Apesar disso, desconfiamos das admiráveis propriedades mecânicas do r-OTFT ao observar que, mesmo após a compactação em um tubo de 30 μm de diâmetro, o dispositivo apresentava as mesmas características elétricas que seu equivalente planar. Além disso, ao retirar a amostra da solução de H_2O_2, alguns dispostivos apresentam um "colapso" devido à forças de capilaridade do líquido no seu interior conforme ilustrado na Figura 18. Após esse colapso, o dispositivo retorna ao formato tubular conforme a solução evapora, e as medidas elétricas não acusam danificações nos dispositivos.

4.3 Aplicação em circuitos simples

Conforme reportado nas informações suplementares do artigo publicado (seção 3.2), foi possível associar dois r-OTFTs em configuração de inversor unipolar do tipo p, assim cumprindo o terceiro objetivo específico deste estudo. Este circuito foi fabricado pela utilização do *wire bonder* (Figura 19). Houve o receio de danificar os dispositivos durante a aplicação do *wire bonder*, uma vez que o processo de solda do fio de ouro nos contatos se

Figura 18 – Colapso do r-OTFT durante a secagem imediatamente após o processo de autoenrolamento.

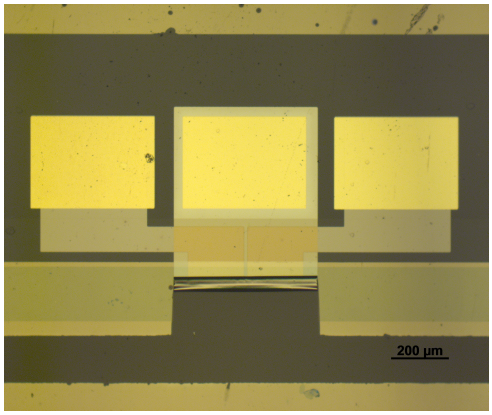

Fonte: o autor (2017)

dá pela aplicação de ultrassom. Tal receio mostrou-se falso, uma vez que foram observados os resultados ilustrados na Figura 11.

Figura 19 – Processo de solda com fios de ouro (*wire bonding*) para a formação de circuitos.

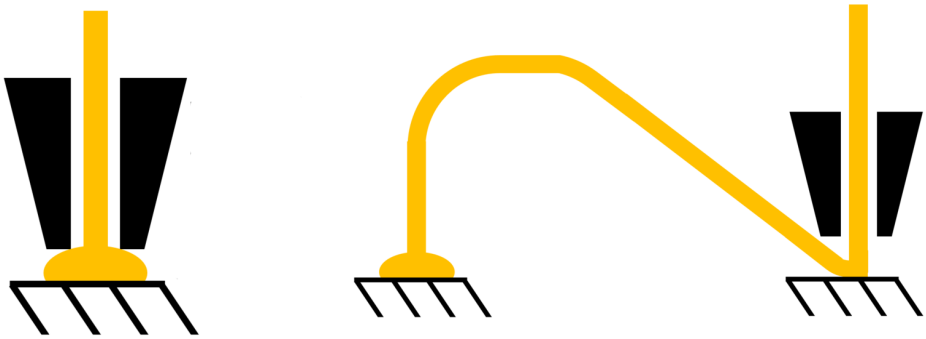

Fonte: adaptado de Hshekhani (2016)

5 CONCLUSÃO

O estudo atingiu o objetivo proposto—produzir transistores orgânicos de filmes finos (OTFTs) ultracompactos, flexíveis e de baixa tensão de operação através da utilização de nanomembranas autoenroladas. Adicionalmente, observou-se propriedades de autoencapsulamento nestes dispositivos devido à alta compactação entre as camadas sucessivas da estrutura tubular—reduzindo a área ativa exposta ao ambiente—possibilitando seu funcionamento em condições agressivas aos semicondutores orgânicos (OSCs). Ou seja, onde os dispositivos tradicionais planares falharam, os rolled-up OTFTs mantiveram sua qualidade de OTFT sem perder a capacidade de detecção destas condições.
Ademais, demonstrando a possibilidade de utilizar diferentes OSCs nesta nova arquitetura—e demonstrando a possibilidade de associar dois ou mais dispositivos em um circuito—abrimos portas para novas aplicações, desde tecnologia aeroespacial até circuitos inteligentes em agricultura.

REFERÊNCIAS

BAGGIO, A. R. et al. Rovibrational spectroscopic constants of the interaction between ammonia and metallo-phthalocyanines: a theoretical protocol for ammonia sensor design. *Physical Chemistry Chemical Physics*, v. 19, n. 17, p. 10843–10853, 2017. ISSN 1463-9076, 1463-9084. Citado 2 vezes nas páginas 43 e 44.

BAO, Z.; LOVINGER, A. J.; DODABALAPUR, A. Organic field-effect transistors with high mobility based on copper phthalocyanine. *Applied Physics Letters*, v. 69, n. 20, p. 3066–3068, nov. 1996. ISSN 0003-6951, 1077-3118. Citado na página 39.

BASIRICÒ, L. et al. Space Environment Effects on Flexible, Low-Voltage Organic Thin-Film Transistors. *ACS Applied Materials & Interfaces*, v. 9, n. 40, p. 35150–35158, out. 2017. ISSN 1944-8244, 1944-8252. Citado 2 vezes nas páginas 25 e 35.

BENDOVA, M. et al. Electrical Properties of Hybrid Nanomembrane/Nanoparticle Heterojunctions: The Role of Inhomogeneous Arrays. *The Journal of Physical Chemistry C*, v. 120, n. 12, p. 6891–6899, mar. 2016. ISSN 1932-7447, 1932-7455. Citado 2 vezes nas páginas 26 e 35.

BROWN, A. et al. Field-effect transistors made from solution-processed organic semiconductors. *Synthetic Metals*, v. 88, n. 1, p. 37–55, abr. 1997. ISSN 03796779. Citado na página 49.

BUFON, C. C. B. et al. Hybrid Organic/Inorganic Molecular Heterojunctions Based on Strained Nanomembranes. *Nano Letters*, v. 11, n. 9, p. 3727–3733, set. 2011. ISSN 1530-6984, 1530-6992. Citado 2 vezes nas páginas 26 e 35.

BUFON, C. C. B. et al. Self-Assembled Ultra-Compact Energy Storage Elements Based on Hybrid Nanomembranes. *Nano Letters*, v. 10, n. 7, p. 2506–2510, jul. 2010. ISSN 1530-6984, 1530-6992. Citado 3 vezes nas páginas 26, 35 e 36.

CHEMICAL SCIENCES AND SOCIETY SUMMIT (CS3), 2012, San Francisco, California, United States. *Organic Electronics for a Better Tomorrow: Innovation, Accessibility, Sustainability*. Citado na página 25.

CHOI, M.-C.; KIM, Y.; HA, C.-S. Polymers for flexible displays: From material selection to device applications. *Progress in Polymer Science*, v. 33, n. 6, p. 581–630, jun. 2008. ISSN 00796700. Citado na página 34.

DAS, R.; HARROP, P. *Printed, Organic & Flexible Electronics Forecasts, Players & Opportunities 2014-2024*. [S.l.]: Sandler Research Market Research Reports Database, 2014. Citado na página 25.

DENG, J. et al. Introducing Rolled-Up Nanotechnology for Advanced Energy Storage Devices. *Advanced Energy Materials*, v. 6, n. 23, p. 1600797, dez. 2016. ISSN 16146832. Citado 2 vezes nas páginas 26 e 35.

DESBIEF, S. et al. Electrolyte-gated organic synapse transistor interfaced with neurons. *Organic Electronics*, v. 38, p. 21–28, nov. 2016. ISSN 15661199. Citado na página 35.

DIMITRAKOPOULOS, C.; MALENFANT, P. Organic Thin Film Transistors for Large Area Electronics. *Advanced Materials*, v. 14, n. 2, p. 99–117, jan. 2002. ISSN 0935-9648, 1521-4095. Citado na página 34.

DING, Z. et al. Effect of Oxygen, Moisture and Illumination on the Stability and Reliability of Dinaphtho[2,3-b:2',3'-f]thieno[3,2-b]thiophene (DNTT) OTFTs during Operation and Storage. *ACS Applied Materials & Interfaces*, v. 6, n. 17, p. 15224–15231, set. 2014. ISSN 1944-8244, 1944-8252. Citado 2 vezes nas páginas 43 e 44.

EGGINGER, M. et al. Current versus gate voltage hysteresis in organic field effect transistors. *Monatshefte für Chemie - Chemical Monthly*, v. 140, n. 7, p. 735–750, jul. 2009. ISSN 0026-9247, 1434-4475. Citado na página 37.

FACCHETTI, A. Semiconductors for organic transistors. *Materials Today*, v. 10, n. 3, p. 28–37, 2007. Citado na página 34.

FARAG, A. Optical absorption studies of copper phthalocyanine thin films. *Optics & Laser Technology*, v. 39, n. 4, p. 728–732, jun. 2007. ISSN 00303992. Citado 4 vezes nas páginas 15, 36, 43 e 52.

FICKER, J. et al. Influence of intensive light exposure on polymer field-effect transistors. *Applied Physics Letters*, v. 85, n. 8, p. 1377–1379, ago. 2004. ISSN 0003-6951, 1077-3118. Citado na página 43.

FORREST, S. R. The path to ubiquitous and low-cost organic electronic appliances on plastic. *Nature*, v. 428, n. 6986, p. 911–918, 2004. Citado na página 34.

FRANSSILA, S. *Introduction to Microfabrication: Franssila/Introduction to Microfabrication*. Chichester, UK: John Wiley & Sons, Ltd, 2010. ISBN 978-1-119-99041-3 978-0-470-74983-8. Citado 2 vezes nas páginas 28 e 29.

FROETER, P. et al. 3d hierarchical architectures based on self-rolled-up silicon nitride membranes. *Nanotechnology*, v. 24, n. 47, p. 475301, nov. 2013. ISSN 0957-4484, 1361-6528. Citado 2 vezes nas páginas 26 e 35.

GRIMM, D. et al. Rolled-up nanomembranes as compact 3d architectures for field effect transistors and fluidic sensing applications. *Nano Letters*, v. 13, n. 1, p. 213–218, jan. 2013. ISSN 1530-6984, 1530-6992. Citado 3 vezes nas páginas 25, 26 e 35.

GUO, X. et al. Current Status and Opportunities of Organic Thin-Film Transistor Technologies. *IEEE Transactions on Electron Devices*, v. 64, n. 5, p. 1906–1921, maio 2017. ISSN 0018-9383, 1557-9646. Citado 2 vezes nas páginas 34 e 35.

HAN, S.-J. et al. High-speed logic integrated circuits with solution-processed self-assembled carbon nanotubes. *Nature Nanotechnology*, v. 12, n. 9, p. 861–865, jul. 2017. ISSN 1748-3387, 1748-3395. Citado na página 34.

HENSON, Z. B.; MÜLLEN, K.; BAZAN, G. C. Design strategies for organic semiconductors beyond the molecular formula. *Nature Chemistry*, v. 4, n. 9, p. 699–704, ago. 2012. ISSN 1755-4330, 1755-4349. Citado na página 34.

HOROWITZ, G. Organic field-effect transistors. *Advanced Materials*, v. 10, n. 5, p. 365–377, 1998. Citado na página 34.

HUANG, G.; MEI, Y. Thinning and Shaping Solid Films into Functional and Integrative Nanomembranes. *Advanced Materials*, v. 24, n. 19, p. 2517–2546, maio 2012. ISSN 09359648. Citado 2 vezes nas páginas 26 e 35.

HUANG, S. et al. Tunable Pseudocapacitance in 3d TiO $_{2-\delta}$ Nanomembranes Enabling Superior Lithium Storage Performance. *ACS Nano*, v. 11, n. 1, p. 821–830, jan. 2017. ISSN 1936-0851, 1936-086X. Citado 2 vezes nas páginas 26 e 35.

HUANG, W. et al. On-Chip Inductors with Self-Rolled-Up SiN_x Nanomembrane Tubes: A Novel Design Platform for Extreme Miniaturization. *Nano Letters*, v. 12, n. 12, p. 6283–6288, dez. 2012. ISSN 1530-6984, 1530-6992. Citado 2 vezes nas páginas 26 e 35.

JOHNSON, P.; CHRISTY, R. Optical constants of transition metals: Ti, V, Cr, Mn, Fe, Co, Ni, and Pd. *Physical Review B*, v. 9, n. 12, p. 5056–5070, jun. 1974. ISSN 0556-2805. Citado na página 51.

KIM, M. S. et al. The effect of indirect UV/ozone treatment on pentacene thin film transistors with double-stacked organic gate insulators. *Organic Electronics*, v. 52, p. 295–300, jan. 2018. ISSN 15661199. Citado na página 35.

KLAUK, H. et al. Ultralow-power organic complementary circuits. *Nature*, v. 445, n. 7129, p. 745–748, fev. 2007. ISSN 0028-0836, 1476-4687. Citado na página 49.

KOCH, C.; RINKE, T. J. *Photolithography: basics of microstructuring*. 1st edition. ed. Ulm: MicroChemicals GmbH, 2017. OCLC: 1001341710. ISBN 978-3-9818782-1-9. Citado na página 29.

KUNUGI, Y. et al. Organic Field-Effect Transistor Using Oligoselenophene as an Active Layer. *Chemistry of Materials*, v. 15, n. 1, p. 6–7, jan. 2003. ISSN 0897-4756, 1520-5002. Citado na página 34.

LEYDECKER, T. et al. Flexible non-volatile optical memory thin-film transistor device with over 256 distinct levels based on an organic bicomponent blend. *Nature Nanotechnology*, v. 11, n. 9, p. 769–775, jun. 2016. ISSN 1748-3387, 1748-3395. Citado na página 34.

MARTINEZ-CISNEROS, C. S. et al. Ultracompact Three-Dimensional Tubular Conductivity Microsensors for Ionic and Biosensing Applications. *Nano Letters*, v. 14, n. 4, p. 2219–2224, abr. 2014. ISSN 1530-6984, 1530-6992. Citado 2 vezes nas páginas 26 e 35.

MATOVIC, J.; JAKŠIĆ, Z. Nanomembrane: A New MEMS/NEMS Building Block. In: TAKAHATA, K. (Ed.). *Micro Electronic and Mechanical Systems*. Rijeka: IntechOpen, 2009. cap. 5, p. 61–84. Citado 3 vezes nas páginas 26, 35 e 41.

MELVILLE, O. A.; LESSARD, B. H.; BENDER, T. P. Phthalocyanine-Based Organic Thin-Film Transistors: A Review of Recent Advances. *ACS Applied Materials & Interfaces*, v. 7, n. 24, p. 13105–13118, jun. 2015. ISSN 1944-8244, 1944-8252. Citado 2 vezes nas páginas 36 e 37.

MERCES, L. et al. Long-Range Coherent Tunneling in Physisorbed Molecular Ensembles. *The Journal of Physical Chemistry C*, v. 121, n. 31, p. 16673–16681, ago. 2017. ISSN 1932-7447, 1932-7455. Citado 2 vezes nas páginas 26 e 35.

MÖNCH, I. et al. Rolled-Up Magnetic Sensor: Nanomembrane Architecture for In-Flow Detection of Magnetic Objects. *ACS Nano*, v. 5, n. 9, p. 7436–7442, set. 2011. ISSN 1936-0851, 1936-086X. Citado 2 vezes nas páginas 26 e 35.

MÜLLER, C. et al. Tuning giant magnetoresistance in rolled-up Co–Cu nanomembranes by strain engineering. *Nanoscale*, v. 4, n. 22, p. 7155, 2012. ISSN 2040-3364, 2040-3372. Citado 2 vezes nas páginas 26 e 35.

NÉNON, S. et al. Shelf-life time test of p- and n-channel organic thin film transistors using copper phthalocyanines. *Thin Solid Films*, v. 518, n. 19, p. 5593–5598, jul. 2010. ISSN 00406090. Citado na página 39.

NIKOLKA, M. et al. High operational and environmental stability of high-mobility conjugated polymer field-effect transistors through the use of molecular additives. *Nature Materials*, v. 16, n. 3, p. 356–362, mar. 2017. ISSN 1476-1122, 1476-4660. Citado na página 34.

NOMURA, K. et al. Room-temperature fabrication of transparent flexible thin-film transistors using amorphous oxide semiconductors. *Nature*, v. 432, n. 7016, p. 488–492, nov. 2004. ISSN 0028-0836, 1476-4679. Citado na página 34.

OH, J. Y. et al. Intrinsically stretchable and healable semiconducting polymer for organic transistors. *Nature*, v. 539, n. 7629, p. 411–415, nov. 2016. ISSN 0028-0836, 1476-4687. Citado na página 34.

OLIVEIRA, R. F. de et al. Single-Electron Charging Effects in Hybrid Organic/Inorganic Nanomembrane-Based Junctions. *The Journal of Physical Chemistry C*, v. 122, n. 23, p. 12131–12139, jun. 2018. ISSN 1932-7447, 1932-7455. Citado 2 vezes nas páginas 26 e 35.

OLIVEIRA, R. F. de et al. Water-gated phthalocyanine transistors: Operation and transduction of the peptide–enzyme interaction. *Organic Electronics*, v. 31, p. 217–226, abr. 2016. ISSN 15661199. Citado 2 vezes nas páginas 36 e 39.

PARK, C. B. et al. Flexible electrophoretic display driven by solution-processed organic TFT with highly stable bending feature. *Organic Electronics*, v. 15, n. 12, p. 3538–3545, dez. 2014. ISSN 15661199. Citado na página 34.

PETRINI, P. A. et al. Hybrid nanomembrane-based capacitors for the determination of the dielectric constant of semiconducting molecular ensembles. *Nanotechnology*, v. 29, n. 26, p. 265201, jun. 2018. ISSN 0957-4484, 1361-6528. Citado 2 vezes nas páginas 26 e 35.

REZENDE, S. M. *Materiais e dispositivos eletrônicos.* São Paulo: Editora Livraria da Física, 2004. OCLC: 69940280. ISBN 978-85-88325-27-2. Citado na página 27.

SATO, H. et al. Degradation by ultra-violet light and its mechanism in organic solar cells. *Organic Electronics*, v. 37, p. 386–395, out. 2016. ISSN 15661199. Citado 2 vezes nas páginas 28 e 41.

SCHMIDT, O. G.; EBERL, K. Nanotechnology: Thin solid films roll up into nanotubes. *Nature*, v. 410, n. 6825, p. 168–168, 2001. Citado 2 vezes nas páginas 26 e 35.

SCHOLZ, S. et al. Degradation Mechanisms and Reactions in Organic Light-Emitting Devices. *Chemical Reviews*, v. 115, n. 16, p. 8449–8503, ago. 2015. ISSN 0009-2665, 1520-6890. Citado 2 vezes nas páginas 28 e 41.

SEKITANI, T. et al. Flexible organic transistors and circuits with extreme bending stability. *Nature Materials*, v. 9, n. 12, p. 1015–1022, dez. 2010. ISSN 1476-1122, 1476-4660. Citado 2 vezes nas páginas 41 e 56.

SHARMA, R. et al. Large-Area Rolled-Up Nanomembrane Capacitor Arrays for Electrostatic Energy Storage. *Advanced Energy Materials*, v. 4, n. 9, p. 1301631, jun. 2014. ISSN 16146832. Citado 3 vezes nas páginas 26, 35 e 36.

SHULAKER, M. M. et al. Three-dimensional integration of nanotechnologies for computing and data storage on a single chip. *Nature*, v. 547, n. 7661, p. 74–78, jul. 2017. ISSN 0028-0836, 1476-4687. Citado na página 34.

SIRRINGHAUS, H. 25th Anniversary Article: Organic Field-Effect Transistors: The Path Beyond Amorphous Silicon. *Advanced Materials*, v. 26, n. 9, p. 1319–1335, mar. 2014. ISSN 09359648. Citado 2 vezes nas páginas 27 e 34.

SOLOVEV, A. A. et al. Tunable catalytic tubular micro-pumps operating at low concentrations of hydrogen peroxide. *Physical Chemistry Chemical Physics*, v. 13, n. 21, p. 10131, 2011. ISSN 1463-9076, 1463-9084. Citado 2 vezes nas páginas 26 e 35.

SOLOVEV, A. A. et al. Light-Controlled Propulsion of Catalytic Microengines. *Angewandte Chemie International Edition*, v. 50, n. 46, p. 10875–10878, nov. 2011. ISSN 14337851. Citado 2 vezes nas páginas 26 e 35.

SOMEYA, T.; BAO, Z.; MALLIARAS, G. G. The rise of plastic bioelectronics. *Nature*, v. 540, n. 7633, p. 379–385, dez. 2016. ISSN 0028-0836, 1476-4687. Citado 3 vezes nas páginas 25, 34 e 39.

SU, Y. et al. Insights into the Interfacial Properties of Low-Voltage CuPc Field-Effect Transistor. *ACS Applied Materials & Interfaces*, v. 5, n. 11, p. 4960–4965, jun. 2013. ISSN 1944-8244, 1944-8252. Citado 2 vezes nas páginas 36 e 39.

SUBBARAO, N. V. et al. Organic field-effect transistors as high performance humidity sensors with rapid response, recovery time and remarkable ambient stability. *Organic Electronics*, v. 32, p. 169–178, maio 2016. ISSN 15661199. Citado na página 39.

THURMER, D. J. et al. Nanomembrane-Based Mesoscopic Superconducting Hybrid Junctions. *Nano Letters*, v. 10, n. 9, p. 3704–3709, set. 2010. ISSN 1530-6984, 1530-6992. Citado 2 vezes nas páginas 26 e 35.

TIMMER, B.; OLTHUIS, W.; BERG, A. v. d. Ammonia sensors and their applications—a review. *Sensors and Actuators B: Chemical*, v. 107, n. 2, p. 666–677, jun. 2005. ISSN 09254005. Citado na página 44.

URASINSKA-WOJCIK, B. et al. 1volt organic transistors with mixed self-assembled monolayer/Al2o3 gate dielectrics. *Organic Electronics*, v. 26, p. 20–24, nov. 2015. ISSN 15661199. Citado na página 38.

VERVACKE, C. et al. Three-dimensional chemical sensors based on rolled-up hybrid nanomembranes. *RSC Advances*, v. 4, n. 19, p. 9723, 2014. ISSN 2046-2069. Citado 3 vezes nas páginas 25, 26 e 35.

VIJAYAN, L. et al. Low power organic field effect transistors with copper phthalocyanine as active layer. *Journal of Science: Advanced Materials and Devices*, v. 3, n. 3, p. 348–352, set. 2018. ISSN 24682179. Citado na página 56.

WANG, J. et al. Fabrication and whispering gallery resonance of self-rolled up gallium nitride microcavities. *Thin Solid Films*, v. 627, p. 77–81, abr. 2017. ISSN 00406090. Citado 2 vezes nas páginas 26 e 35.

WANG, X. et al. Engineered nanomembranes for smart energy storage devices. *Chem. Soc. Rev.*, v. 45, n. 5, p. 1308–1330, 2016. ISSN 0306-0012, 1460-4744. Citado 2 vezes nas páginas 26 e 35.

WATSON, C. et al. Interface state contribution to the photovoltaic effect in organic phototransistors: Photocapacitance measurements and optical sensing. *Organic Electronics*, v. 52, p. 79–88, jan. 2018. ISSN 15661199. Citado na página 43.

YU, X. et al. Ultra-Small, High-Frequency, and Substrate-Immune Microtube Inductors Transformed from 2d to 3d. *Scientific Reports*, v. 5, p. 9661, abr. 2015. ISSN 2045-2322. Citado 2 vezes nas páginas 26 e 35.

ZA'ABA, N. K.; MORRISON, J. J.; TAYLOR, D. M. Effect of relative humidity and temperature on the stability of DNTT transistors: A density of states investigation. *Organic Electronics*, v. 45, p. 174–181, jun. 2017. ISSN 15661199. Citado 2 vezes nas páginas 44 e 56.

ANEXOS

ANEXO A – PAPER REUSE PERMISSION

ACS Publications
Most Trusted. Most Cited. Most Read.

Title: Low-Voltage, Flexible, and Self-Encapsulated Ultracompact Organic Thin-Film Transistors Based on Nanomembranes

Author: Kleyton Torikai, Rafael Furlan de Oliveira, Davi H. Starnini de Camargo, et al

Publication: Nano Letters

Publisher: American Chemical Society

Date: Sep 1, 2018

LOGIN

If you're a copyright.com user, you can login to RightsLink using your copyright.com credentials.

Already **a RightsLink user** or want to learn more?

PERMISSION/LICENSE IS GRANTED FOR YOUR ORDER AT NO CHARGE

This type of permission/license, instead of the standard Terms & Conditions, is sent to you because no fee is being charged for your order. Please note the following:

- Permission is granted for your request in both print and electronic formats, and translations.
- If figures and/or tables were requested, they may be adapted or used in part.
- Please print this page for your records and send a copy of it to your publisher/graduate school.
- Appropriate credit for the requested material should be given as follows: "Reprinted (adapted) with permission from (COMPLETE REFERENCE CITATION). Copyright (YEAR) American Chemical Society." Insert appropriate information in place of the capitalized words.
- One-time permission is granted only for the use specified in your request. No additional uses are granted (such as derivative works or other editions). For any other uses, please submit a new request.

BACK CLOSE WINDOW

Copyright Clearance Center RightsLink® Home Create Account Help

ACS Publications Most Trusted. Most Cited. Most Read.

Title: Low-Voltage, Flexible, and Self-Encapsulated Ultracompact Organic Thin-Film Transistors Based on Nanomembranes

Author: Kleyton Torikai, Rafael Furlan de Oliveira, Davi H. Starnini de Camargo, et al

Publication: Nano Letters

Publisher: American Chemical Society

Date: Sep 1, 2018

LOGIN

If you're a copyright.com user, you can login to RightsLink using your copyright.com credentials.

Already **a RightsLink user** or want to learn more?

Quick Price Estimate

Permission for this particular request is granted for print and electronic formats, and translations, at no charge. Figures and tables may be modified. Appropriate credit should be given. Please print this page for your records and provide a copy to your publisher. Requests for up to 4 figures require only this record. Five or more figures will generate a printout of additional terms and conditions. Appropriate credit should read: "Reprinted with permission from {COMPLETE REFERENCE CITATION}. Copyright {YEAR} American Chemical Society." Insert appropriate information in place of the capitalized words.

I would like to...	reuse in a Thesis/Dissertation
Requestor Type	Author (original work)
Portion	Full article
Format	Print and Electronic
Will you be translating?	No
Select your currency	USD - $
Quick Price	Click Quick Price

QUICK PRICE CONTINUE

This service provides permission for reuse only. If you do not have a copy of the article you are using, you may copy and paste the content and reuse according to the terms of your agreement. Please be advised that obtaining the content you license is a separate transaction not involving Rightslink.

To request permission for a type of use not listed, please contact the publisher directly.